UC San Diego

UC San Diego Electronic Theses and Dissertations

Title

Modeling Hypoplastic Left Heart Syndrome Morphology for Statistical Shape and Biomechanics Analysis

Permalink

https://escholarship.org/uc/item/95p5199d

Author

Tang, Renxiang

Publication Date

2022

Peer reviewed|Thesis/dissertation

eScholarship.org Powered by the California Digital Library
University of California

UNIVERSITY OF CALIFORNIA SAN DIEGO

Modeling Hypoplastic Left Heart Syndrome Morphology for Statistical Shape and Biomechanics Analysis

A Thesis submitted in partial satisfaction of the requirements for the degree Master of Science

in

Bioengineering

by

Renxiang Tang

Committee in charge:

Professor Andrew D. McCulloch, Chair
Professor Francisco Contijoch
Professor Sanjeet Hegde
Professor Jeffrey H. Omens

2022

Copyright

Renxiang Tang, 2022

All rights reserved

The thesis of Renxiang Tang is approved, and it is acceptable in quality and form for publication on microfilm and electronically.

University of California San Diego

2022

DEDICATION

Dedicated to my beloved parents for supporting my pursuit for higher education and for encouraging me to explore different possibilities.

TABLE OF CONTENTS

LIST OF FIGURES

LIST OF TABLES

ACKNOWLEDGEMENTS

I would like to acknowledge and thank my primary advisors, Dr. Andrew McCulloch and Dr. Jeffrey Omens, for their guidance and constant feedback to help me improve in all aspects as a graduate researcher. I would also like to acknowledge my clinical advisors, Dr. Sanjeet Hegde and Dr. James Perry for guiding my project with real clinical impact. I'm also grateful for having Dr. Francisco Contijoch as an advisor on my thesis committee and for all the feedback I've collected along the way.

I would also like to acknowledge may others whose previous work laid the foundation of my thesis projects. I would like to acknowledge and thank Dr. Alistair Young for all the advice during subgroup meetings. I would like to thank Charlène Mauger for her effort in helping with template subdivision. I'm also very grateful for many staff at Rady's Children's Hospital, Fernando Ramirez for uploading data and Robyn Augustyn for manually segmenting data.

I would like to acknowledge the members of Cardiac Mechanics Research Group for the welcoming work environment and constant support. The positivity and fun conversations in lab make a challenging day of research more manageable. I'm truly grateful for having Sachin Govil as my graduate mentor and everything he has done from day 1 to guide me on my research. Thank you for reading my very rough draft of writing, for directing me to resources, for cheering for my progress and for being a supportive climbing friend.

I would like to acknowledge my family and friends for the unconditional love and support through the journey. I would like to acknowledge my parents, Jianming Tang and Yafeng Gao, for always support my pursuit of knowledge, education and pushing boundaries (in good ways). I'm grateful for my aunt and my uncle, Xia Qu and Baoxi Gao, for taking good care of me in the past year and keeping me accompanied. I would like to acknowledge friends for

supporting me through the ride of graduate school and for celebrating the wonderful view after the hardest climbs.

Material in the methods and results sections, in part, has been submitted for International Mechanical Engineering Congress & Exposition (IMECE) 2022. Tang, Renxiang; Govil, Sachin; Mauger, Charlène; Hegde, Sanjeet; Omens, Jeffrey H.; Perry, James C.; McCulloch, Andrew D. "Modeling Single Ventricle Morphology with a HLHS-specific Biventricular Template to Enhance Statistical Shape and Biomechanics Analysis." Thesis author is the primary author of the paper.

ABSTRACT OF THE THESIS

Modeling Hypoplastic Left Heart Syndrome Morphology for Statistical Shape and Biomechanics Analysis

by

Renxiang Tang

Master of Science in Bioengineering

University of California San Diego, 2022

Professor Andrew D. McCulloch, Chair

Modeling the hearts of patient with hypoplastic left heart syndrome (HLHS) has remained an ongoing challenge due to its unique single ventricular morphology. Severe distortions have been observed when using generic biventricular shape templates to create three-dimensional models of HLHS anatomy, which can lead to inaccurate or unconverged numerical analysis. Thus, in this work, we developed a HLHS-specific biventricular template to capture single ventricle morphology in this cohort more accurately and robustly. We applied the HLHS-

specific template to reconstruct HLHS patient-specific models from cardiac magnetic resonance images. Models created using the HLHS-specific template resulted in significantly higher accuracy compared with using the generic template to model the same cohort of patients. The models created using the cohort-specific template were also qualitatively more anatomically realistic with the size of left ventricle and relative location of the apex well captured. When patient-specific models are used for finite element analysis of biomechanics or electrophysiology, it is important to ensure that all elements in the mesh are within an acceptable level of distortion. Element distortion metrics, element edge angles and aspect ratios, confirmed that element distortion in meshes created using the HLHS-specific template is comparable with that of biventricular anatomic models previously used in finite element analysis. A semi-automated workflow, developed to use HLHS-specific template to create patient-individual models from manually segmented contours, will allow future users to create 3D models consistently and efficiently. Accurate 3D patient-specific models will serve as useful tools for statistical shape and physiological analysis to provide insights into new associations between ventricular morphology and clinical outcomes.

1. INTRODUCTION

1.1. Overview of Hypoplastic Left Heart Syndrome

Hypoplastic Left Heart Syndrome (HLHS) is a congenital heart defect (CHD) where structures in the left heart are underdeveloped. HLHS has an occurrence rate of 2 to 3 cases per 10,000 newborns in the United States, and accounts for 1.4% to 4.1% of all congenital heart disease cases [1]. However, despite its relatively low incidence, HLHS accounts for 25-40% of all neonatal cardiac death occurring within the first week of life [2], [3].

The exact cause of HLHS remains to be understood. Several genes have been associated with HLHS, but no consistent markers have been proven. Additionally, no geographical and ethnicity factors have been associated with HLHS, but a 3:2 male to female predominance of prevalence of HLHS has been reported [4].

HLHS can be diagnosed via fetal echocardiogram as early as 18 weeks of pregnancy [5]. However, in one study, only approximately 39% of confirmed HLHS cases were diagnosed prenatally because variants in the cardiac defects make recognizing abnormal anatomical features *in utero* challenging [5]. HLHS can also be diagnosed after birth. Even though babies with HLHS are commonly in good condition at birth, there is a wide spectrum of clinical presentation depending on the underlying anatomical defects. On one end of the spectrum, patients with a wide open ductus arteriosus have uncontrolled pulmonary blood flow and develop signs of congestive heart failure with cardiomegaly due to volume overload [3]. On the other end of the spectrum, patients with a restricted ductus arteriosus are cyanotic and tachycardic [3]. Patients with moderate-sized ductus and coarctation may only develop signs of cyanosis and congestive heart failure after the ductus begins to close [3].

Hypoplastic left heart syndrome comprises a wide spectrum of cardiac malformations characterized by hypoplasia of the left ventricle (LV), aortic valves and mitral valves [6]. Three most common subtypes of HLHS include aortic and mitral stenosis, aortic atresia with mitral atresia, and aortic and mitral atresia [7]. The aortic and mitral atresia subtype with no LV output is the most extreme forms of HLHS. Moreover, HLHS subtypes are also associated with various clinical phenotypes of HLHS, which include slit-like LV, globular LV, and miniature LV. All the cardiac malformations impair blood supply from the left ventricle to the rest of the body affecting both the pulmonary and systemic circulation. Thus, HLHS in an infant without timely intervention is invariably fatal.

The current treatment regime for patients with hypoplastic left heart syndrome is staged palliative surgical treatment consisting of a stage I Norwood procedure at birth, a stage II bidirectional Glenn operation at 4 to 6 months of age, and a stage III Fontan operation at 18 to 48 months of age [8].

1.2. Palliative Treatment of Hypoplastic Left Heart Syndrome

1.2.1. Stage I Palliative Treatment: Norwood Procedure or Hybrid Procedure

The goal of Norwood procedure is to reconstruct the right ventricle (RV) into the dominant pumping ventricle to support systemic circulation [9]. To achieve the goal, multiple reconstruction steps are performed: 1) removal of the atrial septum to ensure sufficient blood flow to the right ventricle, 2) creation of neoaorta by sewing the main branch of pulmonary artery to the underdeveloped aorta followed by aorta arch patch augmentation, and 3) placement of a systemic-to-pulmonary shunt to be the new source of pulmonary blood flow supply [2], [9], [10]. As an outcome, the RV will provide blood into the reconstructed neoaorta and to the

pulmonary vascular bed at the same time. Ideally, blood pumping to the systemic and pulmonary circulations should be evenly distributed.

Most of the surgical advancements in the Norwood operation are associated with the placement and the material of the systemic-to-pulmonary shunt. Currently, there are two different systemic-to-pulmonary shunts used in clinical practice. The first type of shunt, modified Blalock-Taussig shunt (mBTS), establishes communication between the innominate or subclavian artery and pulmonary artery using a Gore Tex Graft. However, mBTS shunt provides continuous blood flow during systole and diastole into the pulmonary artery, which leads to diastolic run off meaning retrograde blood flow in the descending aorta and pulmonary vascular bed [11], [12]. Coronary steal as a result of diastolic runoff may cause ischemia and poor circulation, which leads to death during the hospitalization post-Norwood procedure or during the inter-stage period.

To overcome limitations of mBTS, the right ventricle to pulmonary artery (RVPA) conduit, also known as Sano shunt, was introduced. The Sano shunt establishes connection between the right ventricle and pulmonary artery to yield a higher diastolic pressure. Stabilized hemodynamics lead to more favorable early-stage clinical outcomes with higher transplantation-free survival rate at 12 months in patients with a Sano shunt [13], [14]. However, the Sano shunt group experienced significantly higher rates of unintended interventions and complications [14]. Scar formation in the right ventricle due to ventriculotomy during placement of the Sano shunt has remained a major concern. Multiple studies have demonstrated that scar formation in the right ventricle is a risk factor for developing ventricular arrhythmias, ventricular pseudoaneurysm at the site of incision, and sudden cardiac death due to reduction in global and regional function of the RV [15]–[18].

In recent years, to reduce the operative risk at an early age, a less invasive surgical approach was introduced as an alternative to the stage I Norwood procedure [19], [20]. This hybrid approach consists of: (1) placement of a stent in the patent ductus arteriosus (PDA) to ensure adequate systemic flow, (2) placement of pulmonary artery bands to prevent excessive pulmonary flow, and (3) balloon atrial septostomy to ensure adequate blood supply to the right ventricle [2]. Survival rate of this hybrid procedure was comparable with that of the Norwood procedure, but more frequent pulmonary reintervention and less pulmonary artery development was reported, which pose new challenges to PA reconstruction at stage II palliation [21], [22].

1.2.2. Stage II Palliative Treatment: The Bidirectional Glenn Operation

The major goal of the Bidirectional Glenn operation is to reduce volume loading on the right ventricle by directing systemic venous return to the lungs *via* the superior cavopulmonary connection [23]. During the Bidirectional Glenn operation, the systemic-to-pulmonary shunt is removed and ligated leading to increased diastolic pressure and coronary perfusion. Additionally, the superior vena cava (SVC) is detached from the RV and connected to the pulmonary artery branches, which reduces end-diastolic volume and ventricular wall stress leading to more efficient ventricular function [2], [24].

Bidirectional Glenn surgery was reported to have an overall survival rate of 73% at 5 years, but HLHS patients were associated with high risk of poor outcomes [25], [26]. Possible reasons include underlying cardiac anomaly, severity of tricuspid regurgitation and low weight at the stage of operation [27].

1.2.3. Stage III Palliative Treatment: Fontan Operation

During the stage II bidirectional Glenn operation, only venous blood flowing from upper body *via* the superior vena cava is redirected to the pulmonary artery. A mixture of venous return

flow from the inferior vena cava in the right atrium results in arterial oxygen saturation of 70% to 90%, which can cause organ failure due to hypoxia [2]. Thus, the goal of the stage III Fontan Operation is to improve oxygenation in systemic blood flow by separating the systemic circulation and the pulmonary circulation. During the procedure, the IVC is disconnected from the right atrium first and then connected to the pulmonary artery using either an intra-atrial tunnel or an extracardiac conduit. In some cases, a fenestration is made to connect the Fontan tunnel to the right atrium to provide additional shunt. Oxygen saturation reaches 95% in non-fenestrated Fontan circulation and >80% in fenestrated Fontan circulations [23].

1.3. Unmet Clinical Need

Though stage I procedures were reported to have a 30-day post operative survival rate of over 90%, current shunting or stenting technique selection is based mainly on resources and experience at the surgical center [19], [28]. The decision often does not consider the wide spectrum of valvular abnormalities and heterogeneity of left ventricular morphologies and function. Thus, the impact of surgical shunt selection and volume loading on ventricular shape, especially after the stage II bidirectional Glenn procedure, remain poorly understood. To the best of our knowledge, there has been no study comparing how mBTS, Sano shunt and PDA stent placement affect ventricle shape and remodeling in patients with HLHS.

1.4. Computational Analysis in Hypoplastic Left Heart Syndrome

Cardiac Magnetic Resonance (CMR) imaging provides useful information to assess postsurgical changes in the cardiovascular system, ventricular and valvular function, and other complications [29]. CMR image segmentation allows extraction of three-dimensional (3D) cardiac anatomical and morphological information, and the process ranges from entirely manual to entirely automated. Complete manual segmentation process is time-consuming, and accuracy

of the segmentation depends on skill level of the operator, which can lead to variances in segmentation between operators. On the other hand, completely automated segmentation can be fast with high repeatability, but robust and reliable automated segmentation relies on large training dataset. However, in the case of rare morphologies, expertise in understanding the disease can greatly improve the accuracy of manual segmentation.

Shape information from multiple image slices and time frames in the cardiac cycle can be integrated by registering a shape template to the segmented contours to create dynamic 3D computational models. Researchers have generated 3D models by fitting subdivision surfaces to contours by optimization and registration [30], [31]. One advantage of this modeling approach is the continuity and resolution of the subdivision surface can be controlled by computational rules rather than explicit constrains [31]. Using subdivision surface control mesh templates to create patient-specific models has been widely used in congenital heart disease [32], [33], [34].

Despite progress in ventricular anatomic modeling, its application to single ventricle patients is an ongoing challenge. Previous studies using a left ventricle model template for diseases with a dominant right ventricle in the case of HLHS did not capture details of ventricular anatomy such as the vestigial LV. In preliminary studies, a generic biventricular template developed from normal morphology was used to create 3D patient specific models [35]. The generic template failed to create accurate HLHS-specific models without severe element distortion. Neither of these template-based methods allowed for accurate modeling of RV-dominant morphologies as seen in HLHS. It's also worth pointing out that single ventricle anatomy should be distinguished from single ventricle physiology. Single ventricle anatomy is caused by malformation of ventricle chamber or atrioventricular valves and is typically associated with more complexities of the outflow tracts and semilunar valves [36]. On the other

hand, single ventricle physiology refers to the situation in which the systemic venous return blood and systemic venous return blood are mixed within the heart. Single ventricle physiology can be a result of single ventricle anatomy or stages of palliation surgeries leading to Fontan procedure. Thus, it's important to create anatomically realistic models for HLHS hearts to support subsequent model-based analysis to characterize and compare the structural heterogeneity and its functional impact presented in the cohort.

1.5. Aims of the Thesis

In this research study, we aimed to develop a biventricular shape template that can capture the morphology of HLHS hearts. We used the new template to create patient-specific models for a small cohort of HLHS patients to demonstrate the feasibility of improved performance in creating accurate and anatomically realistic models. The computational models could be used for future analysis of shape and function to generate insights for better clinical prognosis and disease management.

2. METHODS

2.1. Study Population and Image Acquisition

Cardiac magnetic resonance (CMR) data from 10 HLHS patients were obtained from the imaging database at Rady Children's Hospital San Diego (San Diego, US). All imaging data were de-identified according to Health Insurance Portability and Accountability Act (HIPAA) guidelines and were used with the approval of local institutional review boards (IRB) at the University of California San Diego (San Diego, CA).

Each subject underwent functional CMR imaging as part of routine clinical practice. Two-dimensional cine images were acquired using steady-state free precession imaging. Short axis slices (SAX) spanning from base to apex and long axis slices (LAX) including two-

chamber, four chamber, LV outflow tract (LVOT) views, and RV outflow tract (RVOT) views were acquired. All CMR images were acquired using 1.5 T magnetic resonance imaging scanners (GE Discover, GE Healthcare, Milwaukee, US).

2.2. Creation of HLHS-specific Biventricular Template and Subdivision Surfaces

To obtain an HLHS-specific biventricular template, a previously characterized generic biventricular template was interactively registered onto computed tomography (CT) data from a representative HLHS patient [35]. The manual fitting process was performed on the epicardium, RV endocardium and LV endocardium to obtain an anatomically realistic and cohort representative template using Blender (www.blender.org). The resulting biventricular template was subjected to a previously described subdivision surface scheme to obtain a HLHS-specific biventricular mesh [31], [37].

2.3. Image Segmentation

CMR Image segmentation was performed using *cvi42* post-processing software (Circle Cardiovascular Imaging Inc., Calgary, Alberta, Canada). Contours of the endocardial and epicardial layer of both ventricles were manually placed on at least four short axis slices spanning from the most apical to the most basal slice. Additionally, endocardial and epicardial contours were also placed on at least two long axis slices including the four-chamber, left ventricle outflow track and right ventricle outflow track views. All four valves and LV apex were defined on the long axis slices. The contouring process was repeated for both the end-diastolic (ED) and end-systolic (ES) frames. The ED frame was defined as the frame with the largest LV blood pool area and the ES frame was defined as the frame in with the smallest LV blood pool area. The software workspace containing the contours was exported as XML format and the associated CMR images where contours were being placed were exported in the format of digical

imaging and communications in medicine (DICOM). Manual data segmentation was performed by an experienced clinical technologist at Rady Children's Hospital.

2.4. Information Extraction from Contours

The information extraction process parsed the information contained in the manual segmentation and DICOM images and prepared image-related inputs for future steps in the patient-specific modeling. CMR images were first processed to extract information regarding image series and slice number, timeframe, image orientation, image position and pixel spacing using the Pydicom library of the Python lanugage (Python Software Fondation, version 2.3.0).

The contours workspace was first processed using an XML parser of the Python language (Lib/xml/etree/ElementTree.py) to extract information regarding point coordinates, contour types labeled, frame ID and time frame at which each contour was placed. Additional landmarks where the RV freewall joined the inter-vetnricular septum were defined as RV insertion points. Contour labeling of the RV freewall and RV septum were assigned based on the location of RV insertion points. Contour labeling for the all four valves and the apex were defined and updated. All landmark identification and contour updates were performed using a custom Python script to ensure repeatibility and consistency.

2.5. Creation of Patient-specific Models

There were two types of input for guide-point modeling, image-based and template-based. The image-based inputs from manual segmentations and CMR images were described in section 2.4. On the other hand, the template-based input was numerical matrices that characterize the subdivided surface.

The method for creating patient-specific models using guide-point modeling (CIM, Auckland, New Zealand) has been previously described [35], [45]. Briefly, the biventricular

model was iteratively fitted to manually segmented data using a combination of implicit and explicit constraints. First, a 3D template model was initialized by aligning mitral valve, LV apex and interventricular septum landmarks on the template with corresponding landmarks on the manually contoured data. After model initialization, series of linear least-squares fitting (LLS) were first performed to minimize the distance between contour data points and the closest surface point on the template. A D-affine regularization term was used to penalize large mesh deformations [38]. LLS fitting increased computational efficiency for the subsequent diffeomorphic fitting that was perfomed to ensure both anatomically realistic and error-minimized registration. Deformation and displacement of the control mesh template were constrained to ensure the topology of the model was accuractly caputured. For each patient data, the model creation process was performed using the HLHS-specific template and the generic template, respectively. Weights assigned to data points and the template during the fitting process were kept consistent between templates for comparison.

The pipeline from extracting information from manually segmentation and CMR images to using the HLHS-specific template to create patient-specific models is shown in Figure 2.1.

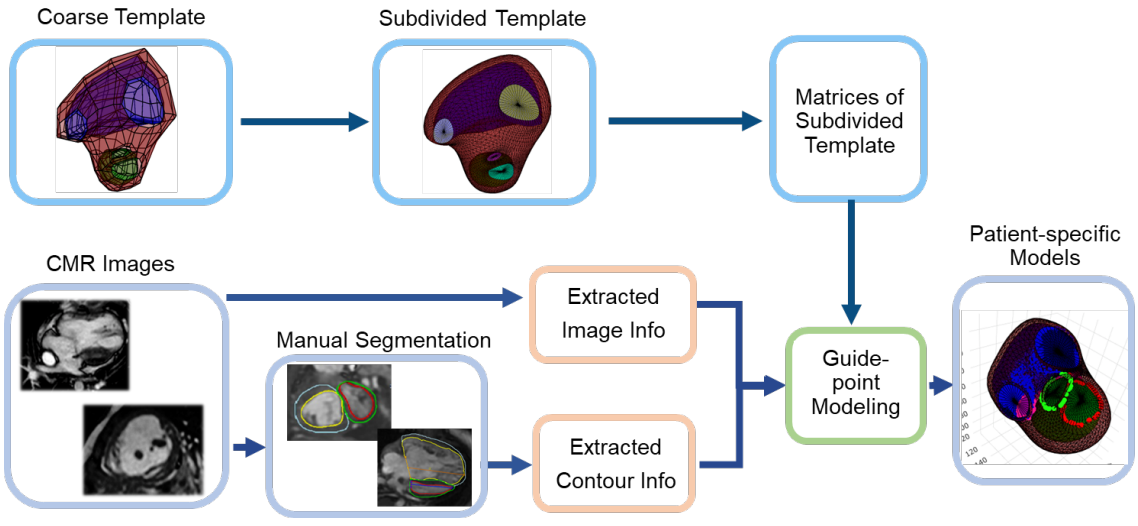

Figure 2.1: Pipeline of processing image input from CMR images and contours, and template input from subdivision surface to create patient-specific models using CIM fitting algorithm

2.6. Characterization of Template Accuracy and Quality

Accuracy was assessed by computing the mean distance between a guide-point on the contours and its closest point on the fitted 3D model surface. Accuracy of using the HLHS-specific subdivision surface as the template to create HLHS patient-specific models were compared with that of using the generic template.

Element edge angle and aspect ratio were commonly used measurements for quantifiying mesh distortion in the context of finite element analysis. To ensure acceptable level of distortion for accurate numerical modeling, for each element in the HLHS-specific template, edge angle was calculated as the maximum angle formed between two adjacent edge and aspect ratio was calculated as the ratio of the longest edge to the shortest edge. The generic template was applied to create a 3D model from normal anatomic data, which has previously demonstrated acceptable levels of distortion for routine finite element analysis [39]. Maximum edge angle and aspect ratio among all elements in the generic normal model were recorded and defined as thresholds for adequate convergence. Correspondingly, when the HLHS-specific template was used to create patient-specific models, the maximum edge angle and aspect ratio of all elements were calculated and compared with the defined threshold. Number of outlying elements was reported. The process was repeated using the generic template to create models for HLHS patients. All edge angle and aspect ratio measurements were performed using the fitted control mesh.

2.7. Statistical Analysis

All statistical analysis was performed using Minitab 17 (http://www.minitab.com/en-US/products/minitab/). Paired t-tests were used to assess the statistical differences in accuracy between templates. Statistical significance was defined at $p < 0.05$.

Material in the methods section, in part, has been submitted for International Mechanical Engineering Congress & Exposition (IMECE) 2022. Tang, Renxiang; Govil, Sachin; Mauger, Charlène; Hegde, Sanjeet; Omens, Jeffrey H.; Perry, James C.; McCulloch, Andrew D. "Modeling Single Ventricle Morphology with a HLHS-specific Biventricular Template to Enhance Statistical Shape and Biomechanics Analysis." Thesis author is the primary author of the paper.

3. RESULTS

3.1. Patient Data and Segmentation

The initial dataset consisted of 10 HLHS patients (1 pre-stage I, 3 pre-stage II and 6 post-stage II). All patients data were segmented and Figure 3.1 depicts the manual contours overlaid on short and long axis images. Three patients were excluded from analysis because they had no visible left ventricle in the CMR images, which was inconsistent with the requirement for model initialization in the guide-point modeling process. Additionally, 1 patient had only one slice of short axis image segmented, which would affect the accuracy of the model due to lack of data and was excluded from further analysis.

The final dataset consisted of 6 HLHS patients (1 pre-stage I, 3 pre-stage II and 2 post-stage II) ranging from mildly hypoplastic to severely hypoplastic with diminished LV systemic function; mild to moderate tricuspid regurgitation was reported in all patients. Demographic information and clinical measurements of cardiac function for all 6 HLHS patients are summarized in Tables 3.1 and 3.2, respectively.

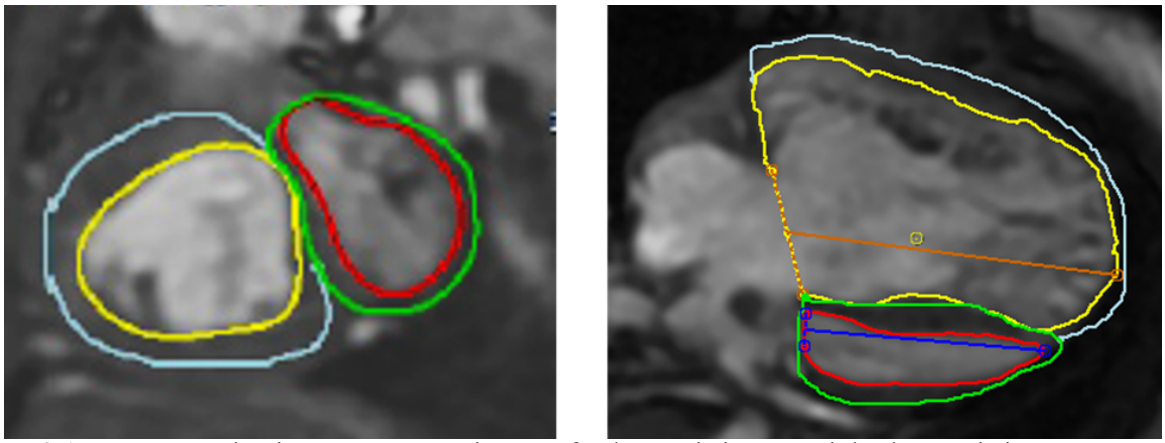

Figure 3.1: Representative image segmentations. Left: short axis image; Right: long axis image. Representation of Image Segmentation. Left: short axis image; Right: long axis image. (Yellow: RV Endocardial Contour, Light Blue: RV Epicardial Contour, Red: LV Endocardial Contour, Green: LV Epicardial Contour, Dark Blue: LAX LV Extent for labeling mitral valve and LV apex; Orange: LAX RV Extent for labeling tricuspid valve)

Table 3.1: Population Demographics

Case	Stage of Palliation Treatment	Shunt Selection during Stage I Treatment	Age of Prior Stage Completion	Age of MRI Scan Acquisition
1	Pre-Stage I	N/A	N/A	5 days
2	Pre-Stage II	mBTS	17 days	87 days
3	Pre-Stage II	Sano	8 days	119 days
4	Pre-Stage II	mBTS	6 days	139 days
5	Post-Stage II	PDA	4 months 16 days	1 year 6 months 11 days
6	Post-Stage II	PDA	4 months 27 days	4 years 1 month 21 days

Table 3.2: Patient Clinical Measurements and Diagnosis

Case	LV Mass (g)	RV Mass (g)	LV EDV (mL)	LV ESV (mL)	LV EF	RV EDV (mL)	RV ESV (mL)	RV EF	Clinical Diagnosis
1	8.2	6.5	8.2	3.6	56%	22.2	8.2	63%	Mildly hypoplastic with severely diminished LV systolic function
2	5.6	15	3.7	1	73%	19.4	14	28%	Severely hypoplastic with normal LV systolic function
3	2.7	16	2.6	2.1	19%	44	25	43%	Severely hypoplastic with severely diminished LV systolic function
4	15	15	20	9	55%	30	14	53%	Mildly hypoplastic with low-normal LV systolic function
5	8	37	1.4	0.9	36%	58	26	55%	Severely hypoplastic with severely diminished LV systolic function
6	15	40	8	6.5	19%	99	44	56%	Severely hypoplastic with severely diminished LV systolic function

3.2. Creation of HLHS-specific Biventricular Template and Subdivision Surfaces

CT scans of a representative HLHS patient at post-Stage II bidirectional Glenn operation were acquired in a patient who was 5 year and 8 months old at the time. The patient had a globular LV with the LV apex near the mid-ventricular plane as shown in Figure 3.2.

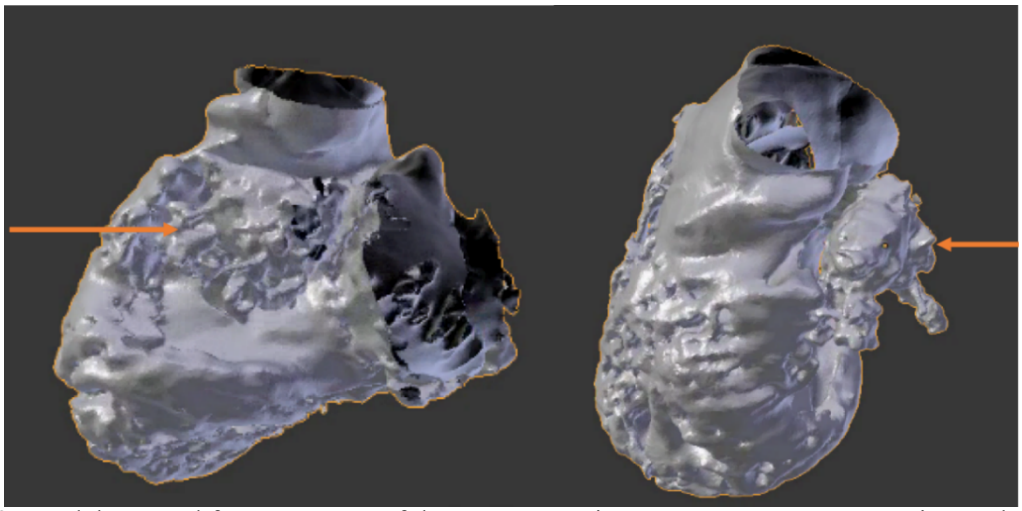

Figure 3.2: Model Created from CT Data of the Representative HLHS Post-Stage II Patient Selected for Template Creation (Orange arrow: location of LV)

The HLHS-specific biventricular template was successfully created by manually registering the epicardium, LV endocardium and RV endocardium layer of the generic biventricular template on CT data of the examplar HLHS patient. The resulting template had 388 vertices and 187 elements that sufficiently characterized single ventricle morphology with the inclusion of all four valves as shown in Figure 3.3 (top row).

The template was successfully subdivided twice using the Catmull-Clark subdivision method, and a HLHS-specific biventricular subdivision surface with 5,810 vertices was generated as shown in Figure 3.3 (bottom row). Additionally, during the subdivison process, matrixes characterizing the subdivided HLHS-specific surface along the circumferential, transmural and longitudinal directions were generated.

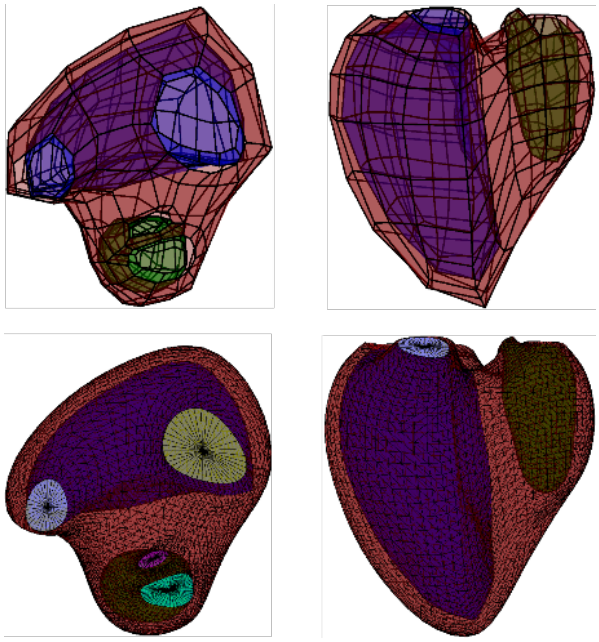

Figure 3.3: The HLHS-specific template. Top row: Coarse template; Bottom row: subdivision surface after Catmull-Clark subdivision

3.3. Creation of Patient-specific Models

A total of 6 HLHS patients with sufficient number of manually segmented contours was used to test the model generation pipeline. Information in CMR images and contours were

extracted and processed to reconstruct patient surface segmentations successfully. A wide spectrum of HLHS morphology, in terms of shape, relative size and location of the left ventricle, was observed within the 6 patients. To be more specific, 4 patients had a globular shaped LV, 1patient had a miniature LV and 1 patient had an LV close to nomal size. A brief description of the individual heart morphology is given in Table 3.3. Images of the representative morphology are shown in Figure 3.4.

Table 3.3: Description of Ventricular Morphology of Each Case

Case	Stage of Palliation Treatment	Description of Ventricular Morphology
1	Pre-Stage I	Globular left ventricle with apex inferior to the mid-ventricular plane
2	Pre-Stage II	Miniature left ventricle with apex inferior to the mid-ventricular plane
3	Pre-Stage II	Globular left ventricle with apex superior to the mi-ventricular plane
4	Pre-Stage II	Left ventricle size and apex location close to healthy morphology
5	Post-Stage II	Globular left ventricle with apex superior to the mid-ventricular plane
6	Post-Stage II	Globular left ventricle with apex inferior to the mid-ventricular plane

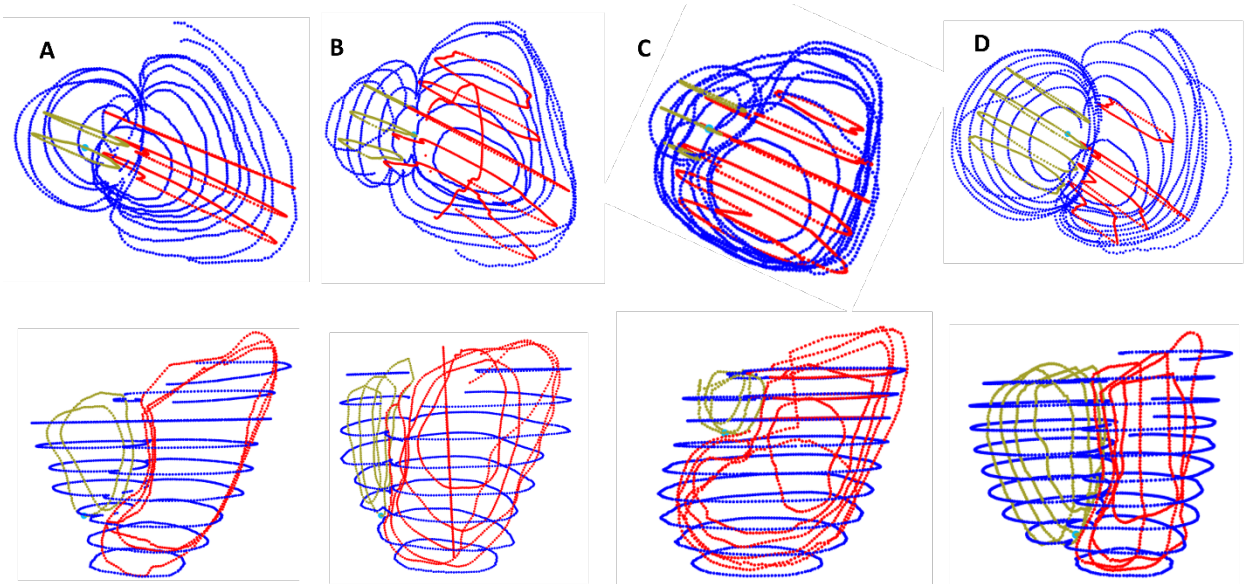

Figure 3.4: Spectrum of HLHS Morphology Presented in the Dataset (Blue: short axis epicardium, Green: long axis RV endocarium, Red: long axis LV endocardium, Light Blue: LV apex point) (A: Case 1, B: Case 2, C: Case 3, D: Case 4)

For each patient at end-diastole, two models were made, one using the generic template and one using the HLHS-specific template. Weights assigned to contour points during the fitting

process were the same for both templates. The fitting process was also repeated for end-systole. Out of the 6 HLHS patients, 5 ED models (Case 1, 2, 3, 5 and 6) and 3 ES (Case 4, 5 and 6) models were succesfully made using both templates, respectively. Other models were failed to be made using both templates due to technical issues during the guide-point modeling process. Figure 3.5 to Figure 3.8 showed the the 3D patient-specific models created using the HLHS-specific template and the generic template for the representative morphology shown above. Refer to appendix for all 8 models created for the dataset.

In the morphology of Case 1 with a globular LV and LV apex inferior to the mid-ventricular plane, the epicardium layer of the model aligned closely with the epicardial contours, and the septum was accurately captured using the HLHS-template as shown in Figure 3.5. Modeling with the generic template caused a basal rotation in the LV, which was not indicated by the manually segmented contours.

In Case 2 with a miniature LV and LV apex inferior to the mid-ventricular plane (Figure 3.6), models made using both templates captured the overall shape of the heart fairly well. However, the LV apex in the model created using the generic template was superior to the location of LV apex marked on the contour, resulting in an elongated LV and distorted anatomy. Additionally, LV bulging was observed in the same model.

In Case 3 with a small globular left ventricle and LV apex point lying superior to the mid-ventricular plane (Figure 3.7), the HLHS template had a slight bend in LV towards to apex, but the RV was closely modeled. On the other hand, the model created using the generic template had significant inward folding towards the apex. The LV was elongated and twisted, deviating from the morphology depicted from the contour.

In Case 4 with an LV slightly smaller than normal (Figure 3.8), both templates captured the overall shape of the ventricles. The model created using the HLHS template resulted in non-smooth epicardium surface around the mitral valve area comparing to that of generic template. However, the model created with the generic template failed to closely capture the apical portion of right venticle resulting in a slight inward folding.

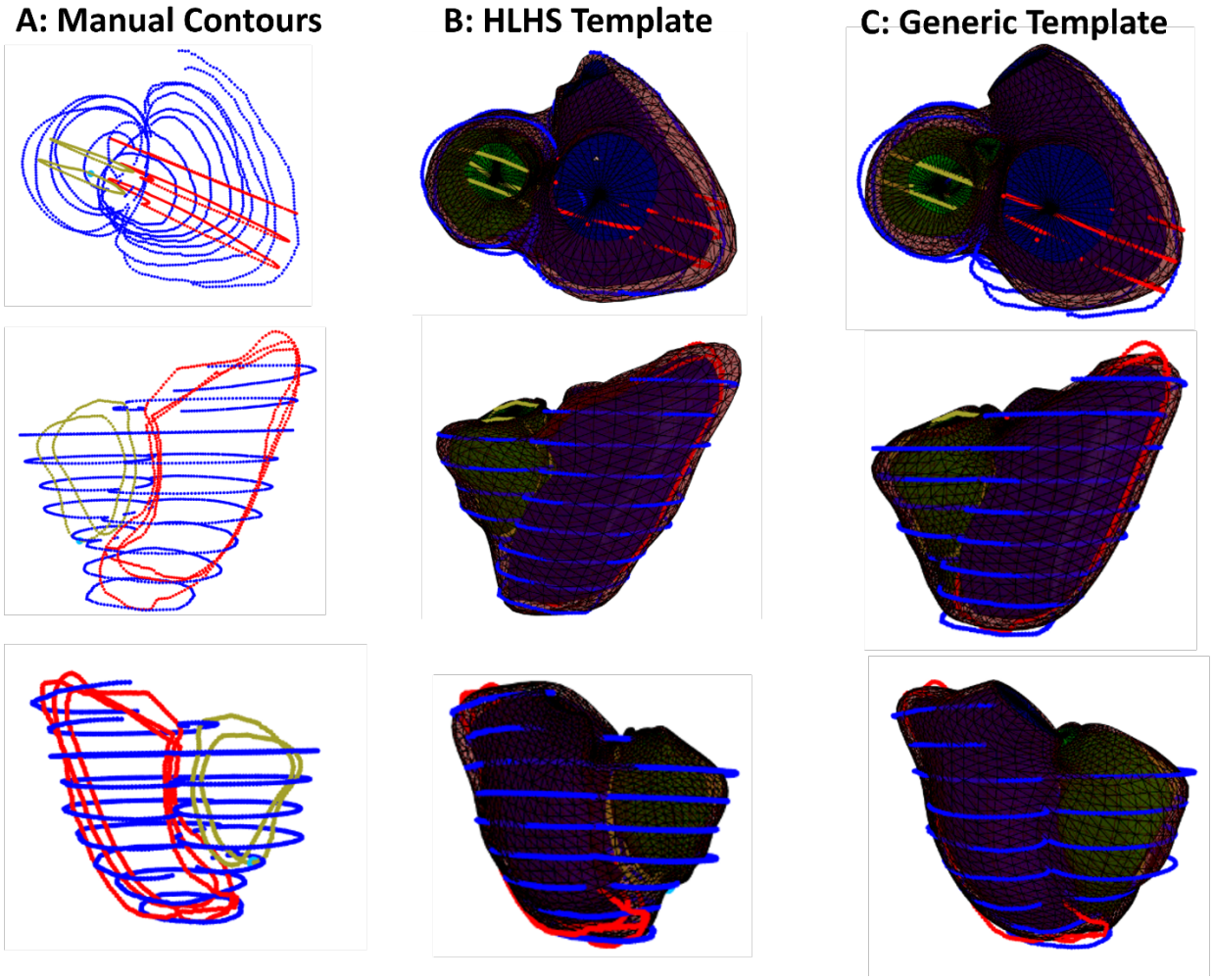

Figure 3.5: Case 1 at End Diastole Models (Blue: epicardium contours, Red: long axis RV endocardium contours, Green: long axis LV endocardium contours, Light Blue: LV apex point)

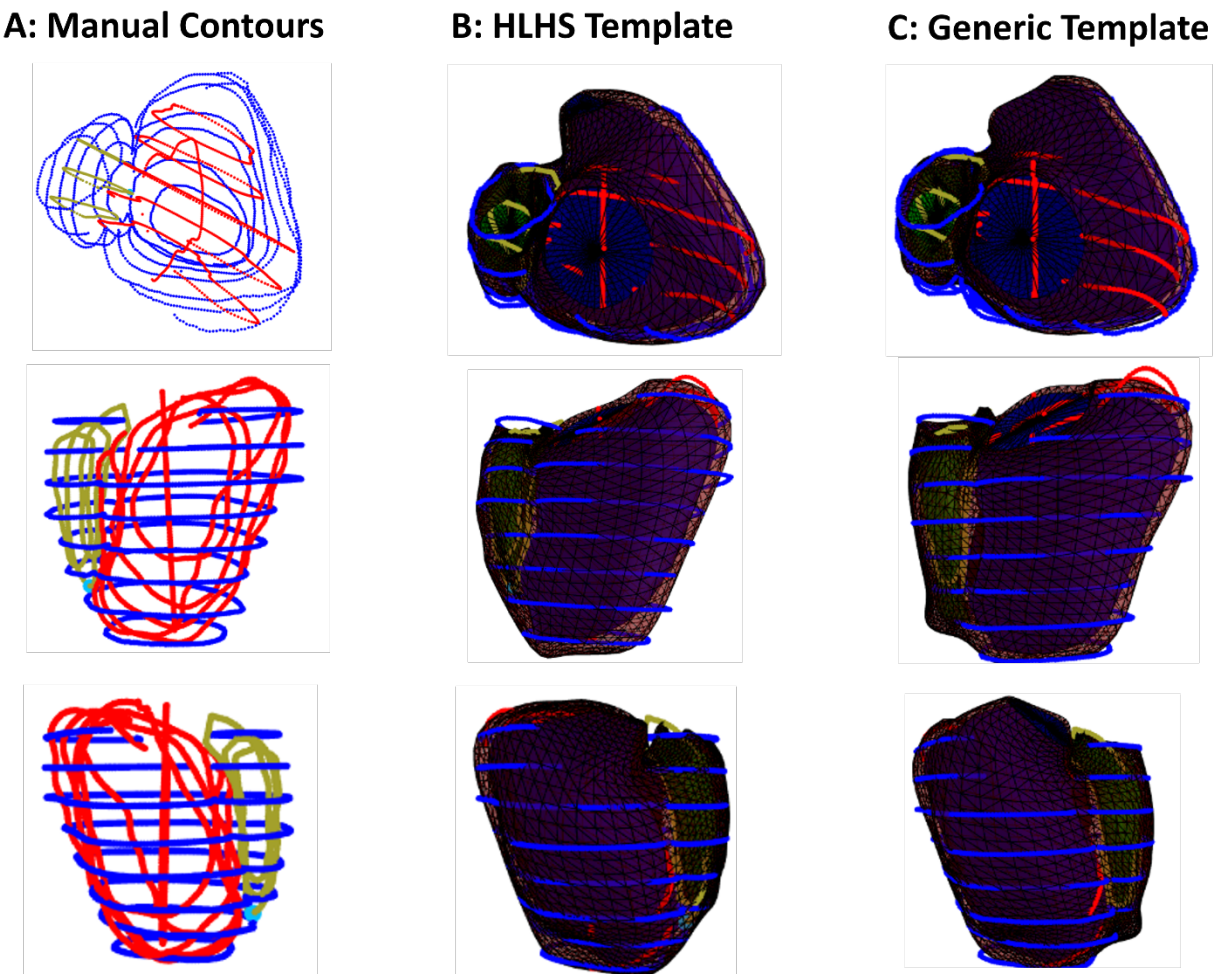

Figure 3.6: Case 2 at End Diastole Models (Blue: epicardium contours, Red: long axis RV endocardium contours, Green: long axis LV endocardium contours, Light Blue: LV apex point)

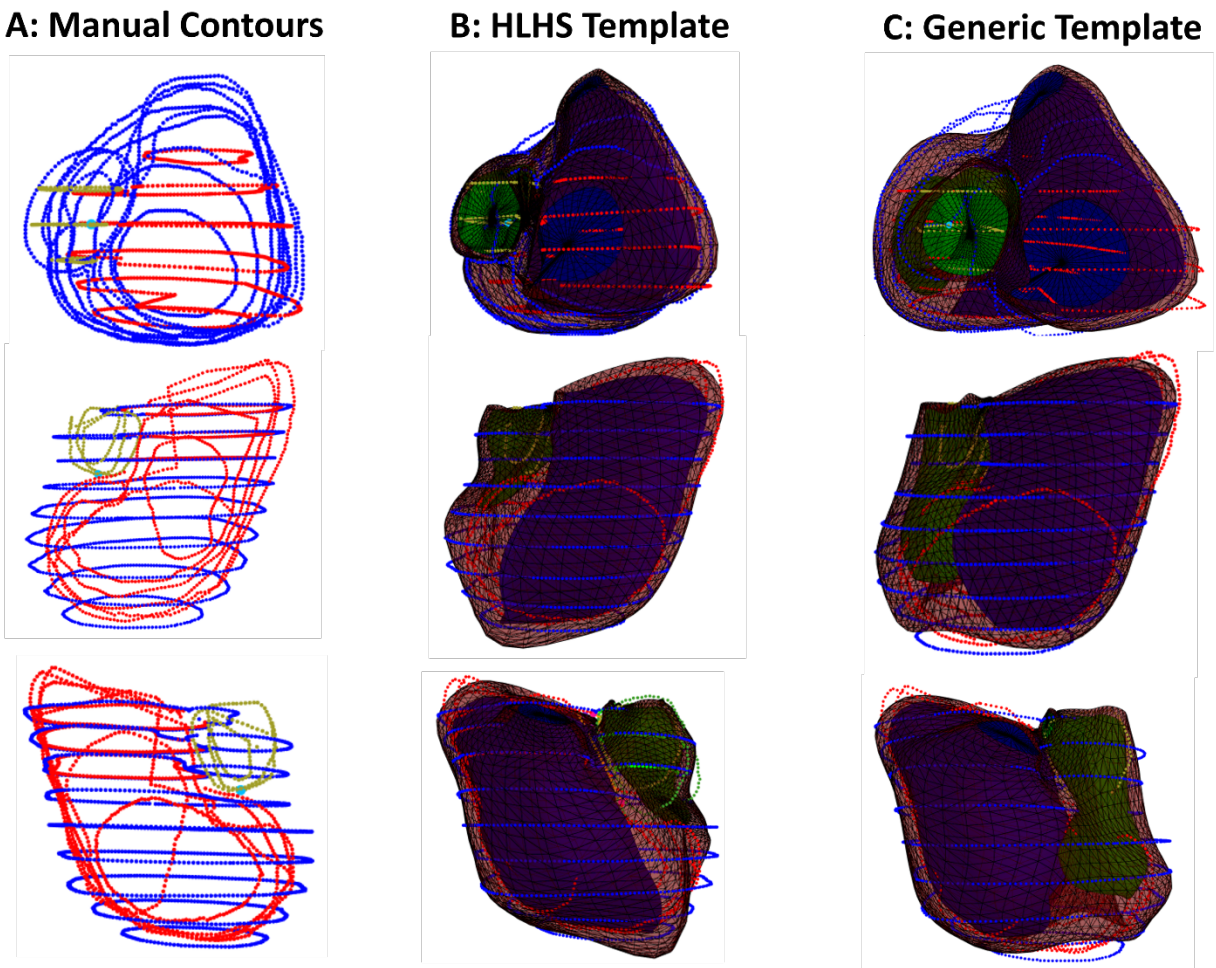

Figure 3.7: Case 3 at End Systole Models (Blue: epicardium contours, Red: long axis RV endocardium contours, Green: long axis LV endocardium contours, Light Blue: LV apex point)

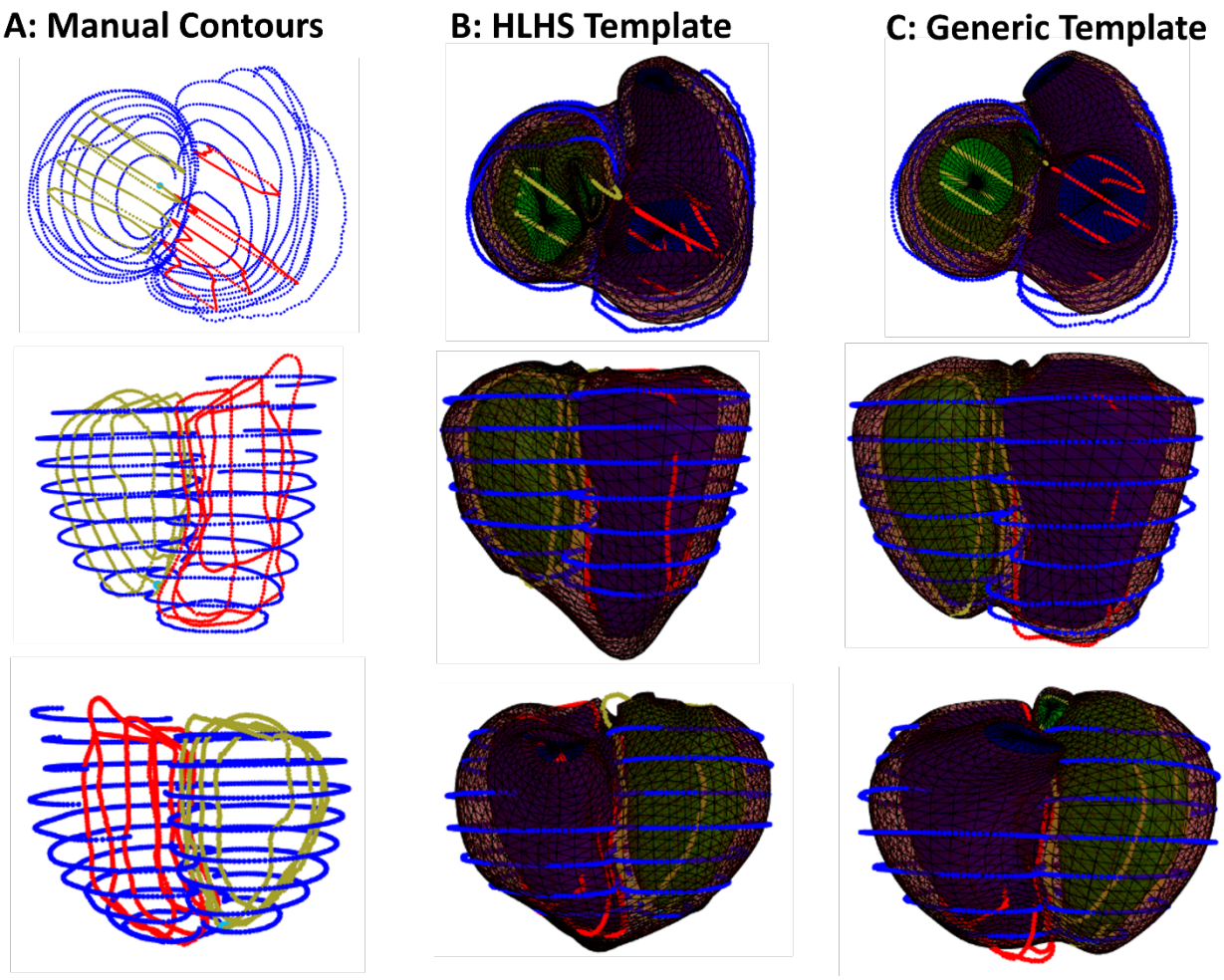

Figure 3.8: Case 4 at End Systole Models (Blue: epicardium contours, Red: long axis RV endocardium contours, Green: long axis LV endocardium contours, Light Blue: LV apex point)

3.4. Template Accuracy Quantification

The accuracy of template was assessed by the mean distance between a guide-point on the contour and the corresponding point on the fitted 3D model. The non-normalized reference mean point-to-point distance was 1.64 mm, which was calculated from using the generic template to create a 3D model for a healthy heart.

To account for the different sizes of the heart, all mean point-to-point measurements were normalized to the cubic root of the total end-diastolic volume (EDV) or end-systolic volume (ESV) depending on the corresponding frame of cardiac cycle. The reference mean point-to-

point of distance was normalized based on average EDV measurements of LV and RV in adult population.

For all 8 models created, the HLHS-specific template had a lower normalized mean point-to-point distance measurements (0.41 ± 0.09) compared with the generic template (0.47 ± 0.10), and this difference was also highly statistically significant ($p = 0.007$). Overall, ED models created had higher accuracy (0.38 ± 0.08) comparing to ES models (0.47 ± 0.09). For a more direct comparison, in Case 5 and 6 where both ED and ES models were successfully created, accuracy for both ED models were higher than that of ES models. Results of template accuracy characterization were summarized in Table 3.4.

Table 3.4: Template Accuracy Characterization

Case	Frame of Cardiac Cycle	Mean point-to-point distance (mm)		Normalized mean point-to-point-distance	
		Generic Template	HLHS-specific Template	Generic Template	HLHS-specific Template
1	ED	1.16	1.08	0.37	0.34
2		1.13	1.12	0.40	0.39
3		1.69	1.59	0.47	0.44
5		2.07	1.78	0.53	0.46
6		1.73	1.27	0.37	0.27
4	ES	1.30	1.18	0.46	0.42
5		1.93	1.71	0.64	0.57
6		1.98	1.48	0.55	0.41
Reference	ED	1.64	N/A	0.27	N/A

3.5. Template Distortion Quantification

Edge angle and aspect ratio of both the HLHS-specific and the generic template were first calculated to characterize the elements of the templates. Maximum edge angle and aspect ratio on each layer of the generic template fitted to a normal heart were defined as thresholds. No edge angle and aspect ratio measurements on the HLHS-specific template were greater than the maximum value on the corresponding generic template layer. Results for template characterization were summarized in Table 3.5 and Table 3.6.

When the template was subjected to create patient-specific models, less distortion was observed in models created using the HLHS-specific template represented by less epicardium inward folding and bulging around LV apex area. Edge angle and aspect ratio for each element on the control mesh of both templates were measured as summarized in Table 3.7 and Table 3.8, respectively. For comparison, maximum edge angle and aspect ratio using the generic template to fit a normal heart were 176.2 degrees and 23.1 and were defined as threshold for quantifying outliers in fitted HLHS meshes. When using the HLHS-specific template to create models, no outliers were identified for both edge angle and aspect ratio, which demonstrated template quality comparable to current standards used for finite element analysis. However, outliers were identified in a total of three models created by the generic template.

Table 3.5: Edge Angle Comparison between Templates

	Generic Template			HLHS-specific Template		
	Average	SD	Max	Average	SD	Max
LV Endocardium	108.95	12.79	143.04	109.58	12.05	142.65
RV Endocardium	111.06	13.25	155.75	112.07	13.77	151.56
Epicardium	110.32	13.93	156.35	110.49	12.75	152.29

Table 3.6: Aspect Ratio Comparison between Templates

	Generic Template			HLHS-specific Template		
	Average	SD	Max	Average	SD	Max
LV Endocardium	1.75	0.96	7.79	1.76	0.66	3.92
RV Endocardium	1.71	0.68	4.54	1.65	0.49	3.50
Epicardium	1.97	1.25	9.07	2.14	1.26	6.65

Table 3.7: Edge Angle Measurements from Patient-specific Model

Case	Frame of Cardiac Cycle	HLHS-specific Template				Generic Template			
		Mean	SD	Max	Number of Outliers	Mean	SD	Max	Number of Outliers
1	ED	118.00	19.80	176.12	0	117.50	16.52	169.41	0
2		125.10	20.18	168.28	0	119.48	17.28	168.42	0
3		123.34	19.83	171.33	0	117.92	19.18	179.44	1
5		117.52	26.90	174.09	0	119.90	19.63	178.37	1
6		119.98	20.86	175.74	0	118.33	16.82	167.29	0
4	ES	119.20	19.89	170.70	0	115.57	16.10	169.44	0
5		124.49	22.77	176.10	0	119.34	18.66	176.16	2
6		121.26	21.27	173.33	0	118.93	19.66	175.62	0

Table 3.8: Aspect Ratio Measurements from Patient-specific Model

Case	Frame of Cardiac Cycle	Generic Template				HLHS-specifc Template			
		Mean	SD	Max	Number of Outliers	Mean	SD	Max	Number of Outliers
1	ED	2.29	1.10	8.52	0	2.52	1.35	8.60	0
2		2.44	1.51	12.94	0	2.56	1.28	11.43	0
3		2.34	1.75	23.49	1	2.66	1.54	12.79	0
5		2.66	2.54	26.70	2	2.96	1.88	15.51	0
6		2.44	1.41	14.12	0	2.77	1.60	17.14	0
4	ES	2.08	1.02	7.97	0	2.54	1.99	18.61	0
5		2.35	1.31	13.10	0	2.58	1.21	9.87	0
6		2.95	1.87	17.65	0	2.90	1.83	13.25	0

Material in the results section, in part, has been submitted for International Mechanical Engineering Congress & Exposition (IMECE) 2022. Tang, Renxiang; Govil, Sachin; Mauger, Charlène; Hegde, Sanjeet; Omens, Jeffrey H.; Perry, James C.; McCulloch, Andrew D. "Modeling Single Ventricle Morphology with a HLHS-specific Biventricular Template to Enhance Statistical Shape and Biomechanics Analysis." Thesis author is the primary author of the paper.

4. DISCUSSION

4.1. Discussion

In this study, we have created a HLHS-specific biventricular template including four valves to capture the morphology of hearts with hypoplastic left heart syndrome. We have characterized the template with respect to quality and accuracy. Using the HLHS-specific template resulted in significantly higher accuracy compared with the generic template for creating patient-specific models for the HLHS cohort. Accuracy of ED models were higher than that of ES models as expected since the template was created based on patient data at ED frame, and this observation was consistent with experience using generic templates to analyze healthy data. Model accuracy at ED and ES measured by point-to-surfaces distances was comparable with existing studies (less than 2 mm non-normalized) [34], [35], [40]. Models created using the HLHS-specific template showed comparable level of distortion to that achieved with the generic template on normal hearts, which is sufficient for finite element analysis [41].

As expected, we observed a wide spectrum of HLHS morphologies in our dataset, especially in terms of the size and relative location of the LV comparing to the RV. The HLHS-specific template demonstrated its versatile application in capturing the morphologies in various HLHS hearts. When taking a closer look at the models, models created for cases with globular LV (Case 1, 3, 5, and 6) demonstrated morphologically realistic models with relatively high accuracy and low distortion. This is because the patient morphology corresponded to the morphology of the representative HLHS patient selected for template creation process. It is worth pointing out that, for comparison, the weights assigned for data fitting were kept consistent for models created with either template. Fitting of HLHS anatomy might be improved by optimizing these weights. Some studies have pointed out that the globular LV is arguably the

most common ventricular morphology presented in the HLHS patient population [42], [43]. The HLHS-specific template demonstrated greater improvement in accuracy when modeling patients with globular LV (15.0%) comparing to non-globular morphology (4.9%). Selection criterion of which template to use primarily depends on the shape of the LV. Additional factors such as ratio of LV and RV mass, ratio of LV and RV volume, and ratio of LV and RV cavity length to quantitatively stratify HLHS patients based on LV shape, size, and relative location of LV apex to determine the template that will generate the most accurate patient-specific models. Additionally, 3 patients with no visible LV were excluded from the study due to incompatibility with the current guide-point modeling process, which relies on LV contours to initialize the model. Thus, accuracy of the template when modeling this particular morphology was not quantified in the current study. However, it is likely that additional templates will be required, especially for patients with no discernible anatomic LV to allow consistent modeling of HLHS morphology.

Based on the data of six patients, patients who received Sano shunts and PDA stents had more globular shaped LV comparing to patients who received mBTS shunts. However, the comparison does not take into account the baseline morphology and, thus, does not provide insight on heart remodeling as a result of shunt selection. With the small sample size of the data available, no conclusion on how shunt selection and different stages of palliative surgery affect heart morphology and function can be drawn. Having longitudinal data of each patient across different stages of the palliative treatment would provide information on establishing connection between shunt selection and heart remodeling. However, another potential reason is that no significant remodeling chances were made at the stage of image acquisition. Previous study has

pointed out that changes in remodeling differences were evident only following stage II Bidirectional Glenn [44].

We were unable to make models for 4 different patient datasets (1 at ED and 3 at ES) due to technical difficulties during the guide-point modeling process. No common characteristic of morphology was observed among the 4 datasets. It's worth pointing out that, for each of the patient, models were failed to be created using both the HLHS-specific template and the generic template, which indicated that the issue was not related to template. The most common problem observed was the template being compressed to align with a particular slice of long axis LV endocardium or long axis RV endocardium. Thus, one potential reason could be associated with the order, in which the templates were aligned and registered to the contours during fitting. Currently, the LV endocardium layer is first registered to the patient data followed by RV freewall, RV septum, epicardium layer, valvular landmarks, and apex.

To the best of our knowledge, this is the first biventricular shape template developed to capture single ventricular morphology in patients with hypoplastic left heart syndrome. Previously, a group of researchers that has reconstructed 3D models for only the right ventricle of HLHS to characterize ventricular remodeling at different stages of the palliative treatment [40], [44]. Besides assuming elliptical shape of the right ventricle, the 3D models were reconstructed only from short axis CMR images, which does not yield the same level of anatomic accuracy as models reconstructed from images of both short axis slices and long axis slices. The RV only models overlooked possible contributions of the vestigial LV to cardiac remodeling, and some workers have pointed out that LV morphology may affect RV function throughout the palliative treatment [45]. Ventricular interactions have also been shown to be associated with the development of tricuspid regurgitation [46]. Thus, the biventricular models

allow the effects of ventricular interactions on structural and functional changes to be modeled in the HLHS patient cohort.

From a clinical perspective, anatomically realistic models ensure clinical decisions are made based on accurate representation of the patient morphology. These models of individual patients can be used to predict patient outcomes, which also can contribute to development of new diagnostic and treatment that tailor to specific cohort of patients.

Additionally, the research project also established a workflow to use the HLHS-specific template to reconstruct 3D patient models from CMR images. Besides the manual segmentation process, the subsequent process of DICOM and contour information processing, linear-least square fitting and diffeomorphic registration were all automated. The semi-automated pipeline will allow future users to process larger amount of segmented image data in a time-efficient manner with greater consistency in model quality. Thus, the creation of the HLHS-specific template and a semi-automated workflow to construct patient-specific models could provide insights to clinical questions that involve anatomical structure and its functional consequences.

4.2. Limitations

The HLHS-specific template was developed based on data of one representative HLHS patient at the stage of post bidirectional Glenn. The manual template development process aimed to reflect the relative size of LV to RV among the HLHS cohort not just to depict the anatomy of an individual patient. However, the process can be subjective given the wide spectrum of HLHS patient anatomy as a result of different stages of the palliative treatment.

The number of slices of manually segmented data could impact the quality of the patient-specific model created. In some patients, the short axis RV endocardium layer was contoured from the most basal slice to the mid-ventricular slice, leaving the mid-ventricular to apical

portion of the RV unconstrained during model fitting. Moreover, manual data segmentation is prone to introducing subjective variance. In the current study, manual segmentation was performed by a clinician with experience performing data segmentation and taking measurements using the image post-processing software, cvi42. However, we acknowledge the accuracy of the contouring process would depend on clinician's understanding of the disease anatomy and information in the imaging dataset. Additionally, manual segmentation is time-consuming, taking the clinician an average two hours to process one set of patient data, which could add additional burden to already busy clinical schedule.

Even though both the aortic and pulmonary valves were manually segmented, they were not modeled in the patient-specific models because the position of the valves was highly variable. Thus, there were no computational constraints on deformation or registration around the valve annuli leading to the epicardium folding around the valve plane in some models. This indicates the need for further improvements to enhance model quality and detail.

The retrospective nature of the clinical portion of the project is another limitation of the study. We experienced challenges posed by CMR image quality during manual data segmentation. Some patients had a missing dataset of short axis slices or image stacks failed to span the whole heart. A potential reason is that the mBTS has been the standard of care for more than 30 years prior to Sano shunts becoming the standard of care in the past decade. Recently, more surgical centers are adopting the less invasive hybrid approach as the standard of care for stage I palliation invasiveness. Both surgical and imaging advancements could alter the availability and quality of CMR data. It would be most ideal to use CMR data of the same patient to compare across different stages of the palliative treatment. However, CMR imaging was not considered part of the clinical standard procedure until more recently, which limits the number of

patients with complete, high-quality CMR images performed across different stages of palliation treatment. Additionally, all patient CMR data were collected at a single surgical center, which could potentially limit the spectrum of HLHS morphology presented.

4.3. Future Work

4.3.1. Template Improvement

To address one of the limitations discussed regarding template creation, the performance of the template can be further improved by incorporating measurements of size and volume of multiple HLHS hearts in the manual registration process. The measurements will provide quantitative metrics to ensure the template reflects the common characteristics presented in the patient cohort. Alternatively, we can use machine learning method to first calculate the average shape of the HLHS hearts with available datasets and subsequently compare the average cohort shape with the current template to make adjustments.

Additionally, 3 out of 10 patients originally selected for the study did not have visible left ventricle in the CMR dataset potentially due to slit-like morphology of the LV, which necessitated a need for a separate single ventricle template to model the morphology accurately and consistently.

4.3.2. Parameter to Quantify Accuracy

Currently, model accuracy was measured by mean point-to-surface distance between the contour data point and the corresponding point on the model surface. However, the measurements only accounted for one side of proximity. Hausdorff distance (HD) is an alternative parameter that measure the distance between two sets of points. HD has been used to evaluate accuracy of medical imaging segmentation and registration in the field of brain tumor segmentation, cerebral vessel segmentation and many more [47]–[49]. In the case of mean point-

to-point distance measurement, the distance of far points can be offset by other near points and required an establishment of one-to-one reference. However, Hausdorff distance is a max-min distance and does not require a one-to-one mapping, which is more sensitive to represent the spatial position of each individual point [47]. Thus, Hausdorff distance will be a useful metric to include for quantifying model registration accuracy since it takes into account both the distance from data points to model surface and model surface to data points. Ventricle volume and mass measurements from the CMR images could be compared to that from the fitted model to quantify accuracy of models created using both templates, which has been done previously [35].

Additionally, it will be helpful to have clinicians compare the DICOM images, segmented contours and models fitted using the HLHS-specific template and the generic template. The comparison aims to gauge clinical insights to subjectively quantify the accuracy of the fitted models and quality of models for clinical decision making.

4.3.3. Quantify Impact of Operator Variance on Template Performance

Manual image segmentation requires operators to have sufficient understanding of the disease morphology to produce accurate and repeatable results. Thus, we need to quantify the impact of operator variance on model accuracy by having operators with various experience levels to perform manual data segmentation following the protocol prepared and edited by clinician. For each patient, contours segmented by different operators will be used to reconstruct patient-specific models using the HLHS-specific template and accuracy of the model will be compared. Sensitivity analysis can be performed to quantify the degree of accuracy of model being impacted by operators' ability to understand HLHS morphology and to manually segment contours correctly as instructed.

4.3.4. Atlas-based Analysis

Atlas-based analysis of CMR images has been used for quantifying changes in ventricular shape in congenital heart diseases [50], [51]. The analysis provides useful insights for congenital heart defect patients with single ventricle morphology comparing with current clinical measurements of evaluating cardiac remodeling and assessing the risk of heart failure [50]. With a large enough dataset of HLHS patients, statistical shape atlases can be constructed for the cohort based on methods described previously [51]. Using principal component analysis (PCA), we can identify shape modes that describe the most important variation within the HLHS population. Subsequently, models of individual HLHS patient can be projected on the cohort atlas, which allows for characterization of how abnormal an individual is relative to the HLHS population.

The atlas-based statistical shape analysis will provide insights on the initial clinical question of how volume loading due to surgical shunt selection affect heart remodeling especially at the stage of post bidirectional Glenn procedure. A previous study has utilized a similar atlas-based analysis to compare the effects of the Sano and mBTS shunts on ventricular shape and function. Two shape modes were identified corresponding to increased sphericity and dilation of the right ventricle in patients who received a Sano shunt compared with mBTS [44]. However, the study did not include the PDA stents group in the comparison, which has recently gained clinical preference at surgical centers. With the hybrid approach being included in the study, we hypothesize that it will take higher number of shape modes to explain the variation in the patient population and each mode will explain less amount of variation within the cohort.

Another important application of the atlas-based analysis is to identify early signs of heart failure after Fontan procedure. Researchers have pointed out that the systemic right

ventricular morphology in HLHS patients is associated with higher long-term mortality and greater risk of heart failure after Fontan surgery [52], [53]. Preservation of RV function is one of the factors that is essential for the success of a Fontan procedure [53]. There are multiple shape features identified to be associated with RV dysfunction including tricuspid valve annular dilation or angulation, changes in RV global shape, and changes in shape of right ventricle outflow tract [52], [53]. Additionally, biomechanical markers including reduction in global and local strain in HLHS could also be another indicator of RV dysfunction [44], [54]. Both shape features and biomechanics markers unique to the cohort could be generated by a large scale longitudinal study of HLHS patients at different stages of the palliative treatment and with different surgical shunt selection during stage I.

Having a HLHS-specific statistical shape atlas will also reduce computational costs by dimensionally reducing complex CMR images into a more compact set of orthogonal shape parameters. An HLHS-specific atlas could add clinical value. Clustering and regression analysis can be performed on shape modes along with traditional clinical measurements. If an association is successfully established, the derived shape metrics and standard clinical measurements can be applied to analysis of individual patients providing for more quantitative and personalized clinical decision making.

5. CONCLUSION

The project originated with the clinical question regarding the relationship between shunt selection during stage I palliative treatment and ventricular shape at the post stage II treatment. There was an unmet need to create accurate and anatomically realistic patient-specific models for of single ventricular morphology in the HLHS patient cohort. Thus, we created a HLHS-specific biventricular shape template by manually registering each layer of the generic template on a

representative HLHS heart. We characterized the newly developed template with respect to accuracy and distortion and demonstrated that the HLHS-specific template can model HLHS morphology with higher accuracy and less mesh distortion than a generic template. The distortion in models created with the HLHS cohort-specific template was comparable with current models of the normal heart used for finite element analysis. To the best of our knowledge, this is the first biventricular shape template created for capturing single ventricular morphology in HLHS hearts.

The new pipeline for model creation involved segmenting CMR images, extracting information from contours, identifying landmarks, and creating patient specific models. The establishment of a semi-automated pipeline will allow future users to process large number of segmented cases efficiently, accurately, and repeatedly.

In conclusion, the research project has created a biventricular shape template based on the single ventricle morphology in HLHS patient. We have also demonstrated the feasibility of using the HLHS-specific template to create more accurate and anatomically realistic models for the patient cohort of interest with less mesh distortion. The work is a foundation for future large scale statistical shape analysis and biomechanical analysis to quantify 3D cardiac structural and functional changes at different stages of the palliative treatment, and to identify early shape and biomechanical markers for predicting heart failure in HLHS patients post-Fontan operation.

6. REFERENCE

[1] R. Javed, F. Cetta, S. M. Said, T. M. Olson, P. W. O'Leary, and M. Y. Qureshi, "Hypoplastic Left Heart Syndrome: An Overview for Primary Care Providers," *Pediatr. Rev.*, vol. 40, no. 7, pp. 344–353, Jul. 2019, doi: 10.1542/PIR.2018-0005.

[2] M. Yabrodi and C. W. Mastropietro, "Hypoplastic left heart syndrome: From comfort care to long-term survival," *Pediatr. Res.*, vol. 81, no. 1–2, pp. 142–149, 2017, doi: 10.1038/pr.2016.194.

[3] D. J. Barron, M. D. Kilby, B. Davies, J. G. C. Wright, T. J. Jones, and W. J. Brawn, "Hypoplastic left heart syndrome," *Lancet*, vol. 374, no. 9689, pp. 551–564, 2009, doi: 10.1016/S0140-6736(09)60563-8.

[4] T. Karamlou, B. S. Diggs, R. M. Ungerleider, and K. F. Welke, "Evolution of treatment options and outcomes for hypoplastic left heart syndrome over an 18-year period," *J. Thorac. Cardiovasc. Surg.*, vol. 139, no. 1, pp. 119–127, Jan. 2010, doi: 10.1016/J.JTCVS.2009.04.061.

[5] S. A. Morris, M. Ethen, D. Penny, M. Canfield, C. Minard, D. Fixler, W. Nembhard "Prenatal diagnosis, birth location, surgical center, and neonatal mortality in infants with hypoplastic left heart syndrome," *Circulation*, vol. 129, no. 3, pp. 285–292, Jan. 2014, doi: 10.1161/CIRCULATIONAHA.113.003711.

[6] R. T. Sadineni, B. S. Kumar, N. Chander, and D. M. Boppana, "Prenatal Sonographic Diagnosis of Hypoplastic Left Heart Syndrome," *Int. J. Appl. Basic Med. Res.*, vol. 7, no. 3, p. 213, 2017, doi: 10.4103/IJABMR.IJABMR_389_16.

[7] D. A. Hayes, W. W. Lai, P. Frommelt, and E. Bacha, "Beyond Hypoplastic Left Heart Syndrome: The Spectrum of Congenital Heart Disease Associated with Left Ventricular Hypoplasia," *Curr. Pediatr. Rep.*, vol. 1, no. 2, pp. 102–108, Jun. 2013, doi: 10.1007/S40124-013-0016-6/FIGURES/1.

[8] P. Richard G. Ohye, MD1, Dietmar Schranz, MD, PhD2, and Yves D'Udekem, MD, "Current Therapy for Hypoplastic Left Heart Syndrome and Related Single Ventricle Lesions," *Physiol. Behav.*, vol. 176, no. 10, pp. 139–148, 2017, doi: 10.1161/CIRCULATIONAHA.116.022816.Current.

[9] W. I. Norwood, J. K. Kirklin, and S. P. Sanders, "Hypoplastic Left Heart Syndrome: Experience with Palliative Surgery," *Am. J. Cardiol.*, vol. 45, no. 1, pp. 87–91, 1980, doi: 10.1016/0002-9149(80)90224-6.

[10] T. Hasegawa, O. Yoshihiro, M.Ayako, M. Hironori, T. Akiko, N. Rei, M. Shunsuke "Aortic arch geometry after the Norwood procedure: The value of arch angle augmentation," 2015, doi: 10.1016/j.jtcvs.2015.05.012.

[11] J. W. Newburger, L. A. Sleeper, P. C. Frommelt, G. D. Pearson, W. T. Mahle, S. Chen, C. Dunbar-Masterson, S. Mital, I. A. Williams, N. S. Ghanayem, C. S. Goldberg, J. P. Jacobs, C. D. Krawczeski, A. B. Lewis, S. K. Pasquali, C. Pizarro, P. J. Gruber, A. M. Atz, S. Khaikin, J.W. Gaynor, R. G. Ohye, "Transplant-free survival and interventions at 6 years in the SVR trial," *Circulation*, vol. 137, no. 21, pp. 2246–2253, 2018, doi: 10.1161/CIRCULATIONAHA.117.029375.

[12] C. Pizarro, R. R. Davies, E, Woodfordm W. A. Radtke, “Right Ventricle to Pulmonary Artery Conduit Improves Outcome After Stage I Norwood for Hypoplastic Left Heart Syndrome,” *Circulation*, vol. 108, no. 10 SUPPL., Sep. 2003, doi: 10.1161/01.CIR.0000087390.94142.1D.

[13] S. G. Raja, “Right ventricle to pulmonary artery shunt modification of Norwood procedure: Outcomes, concerns, and controversies,” *Ann. Pediatr. Cardiol.*, vol. 4, no. 2, p. 150, Jul. 2011, doi: 10.4103/0974-2069.84654.

[14] R. G. Ohye, L. A. Sleeper, L. Mahony, J. W. Newburger, G. D. Pearson, M. Lu, C. S. Goldberg, S. Tabbuttm P.C. Frommelt, N. S. Granayem, P. Laussen, J. F. Rhodes, A. B. Lewis, S. Mital, C. Ravishankar, I. A. Williams, C. Dunbar-Masterson, A. M. Atz, S. Colan, L. L. Minich, C. Pizarro, K. R. Kanter, J. Jaggers, J. P. Jacobs, C. D. Krawczeski, N. Pike, B. W. McCrindle, L. Virzi, J. W. Gaynor, “Comparison of Shunt Types in the Norwood Procedure for Single-Ventricle Lesions,” *N. Engl. J. Med.*, 2010, doi: 10.1056/nejmoa0912461.

[15] S. C. Menon, L. K. Erickson, M. McFadden, and D. V. Miller, “Effect of ventriculotomy on right-ventricular remodeling in hypoplastic left heart syndrome: A histopathological and echocardiography correlation study,” *Pediatr. Cardiol.*, vol. 34, no. 2, pp. 354–363, 2013, doi: 10.1007/s00246-012-0462-x.

[16] E. J. Hall, A. H. Smith, F. A. Fish, D. P. Bichell, B. A. Mettler, K. Crum, P. J. Kannankeril, A. E. Radbill, “Association of Shunt Type With Arrhythmias After Norwood Procedure,” *Ann. Thorac. Surg.*, vol. 105, no. 2, pp. 629–636, Feb. 2018, doi: 10.1016/J.ATHORACSUR.2017.05.082.

[17] S. Takabayashi, H. Shimpo, K. Yokoyama, K. Onoda, and Y. Mitani, “Reduced regional right ventricular wall motion after transventricular repair of tetralogy of Fallot,” *J. Thorac. Cardiovasc. Surg.*, vol. 133, no. 6, pp. 1656–1658, Jun. 2007, doi: 10.1016/J.JTCVS.2007.03.001.

[18] J. Hörera, I. Malcicb, C. Schreibera, and R. Langea, “False aneurysm origination from the proximal anastomosis of a right ventricular to pulmonary artery shunt following staged repair of hypoplastic left heart syndrome,” *Interact. Cardiovasc. Thorac. Surg.*, vol. 12, no. 3, pp. 487–489, Mar. 2011, doi: 10.1510/ICVTS.2010.246009.

[19] M. Kaplinski, R. F. Ittenbach, M. L. hunt, D. Stephan, S. S. Natarajan, C. Ravishankar, T. M. Giglia, J. Rychik, J. J. Rome, M. Mahle, A. T. Kennedy, J. M. Steven, S. C. Nicolson, T. L, Spray, J. William Gaynor, C. E. Mascio, “Decreasing interstage mortality after the norwood procedure: A 30-year experience,” *J. Am. Heart Assoc.*, vol. 9, no. 19, p. 16889, Oct. 2020, doi: 10.1161/JAHA.120.016889.

[20] D. Schranz, “High risk HLHS: hybrid approach yes, but how does it work?,” *Transl. Pediatr.*, vol. 7, no. 3, p. 222, Jul. 2018, doi: 10.21037/TP.2018.07.03.

[21] K. Baba, Y. Kotani, D. Chetan, R. R. Charurvedi, K. J. Lee, L. N. Benson, L. Grosse-Wortmann, G. S. Van Arsdell, C. A. Caldarone, O. Honjo, “Hybrid versus norwood strategies for single-ventricle palliation,” *Circulation*, vol. 126, no. 11 SUPPL.1, Sep. 2012, doi: 10.1161/CIRCULATIONAHA.111.084616.

[22] H. Dave, B. Rosser, W. Knirsch, M. Hübler, R. Prêtre, and O. Kretschmar, “Hybrid approach for hypoplastic left heart syndrome and its variants: the fate of the pulmonary

arteries," *Eur. J. Cardio-Thoracic Surg.*, vol. 46, no. 1, pp. 14–19, Jul. 2014, doi: 10.1093/EJCTS/EZT604.

[23] P. P. Roeleveld, D. M. Axelrod, D. Klugman, M. B. Jones, N. K. Chanani, J. W. Rossano, J. M, Costello, "Hypoplastic left heart syndrome: From fetus to fontan," *Cardiol. Young*, vol. 28, no. 11, pp. 1275–1288, 2018, doi: 10.1017/S104795111800135X.

[24] W. T. Mahle, M. S. Cohen, T. L. Spray, and J. Rychik, "Atrioventricular valve regurgitation in patients with single ventricle: impact of the bidirectional cavopulmonary anastomosis," *Ann. Thorac. Surg.*, vol. 72, no. 3, pp. 831–835, 2001, doi: 10.1016/S0003-4975(01)02893-4.

[25] B. Alsoufi, C. Manlhiot, A. Awan, F. Alfadley, M. Al-Ahmadi, A. Alwadei, B. W. McCrindle, Z. Al-Halees, "Current outcomes of the Glenn bidirectional cavopulmonary connection for single ventricle palliation," *Eur. J. Cardio-Thoracic Surg.*, vol. 42, no. 1, pp. 42–49, Jul. 2012, doi: 10.1093/EJCTS/EZR280.

[26] S. Silvilairat, Y. Pongprot, R. Sittiwangkul, S. Woragidpoonpol, S. Chuaratanaphong, and W. Nawarawong, "Factors influencing survival in patients after bidirectional Glenn shunt," *Asian Cardiovasc. Thorac. Ann.*, vol. 16, no. 5, pp. 381–386, 2008, doi: 10.1177/021849230801600508.

[27] W. F. Carlo, k. E. Carberry, J. S. Heinle, D. L. Morales, E. Dean Mckenzie, C. D. Fraser, D. P, Nelson, "Interstage attrition between bidirectional Glenn and Fontan palliation in children with hypoplastic left heart syndrome," *J. Thorac. Cardiovasc. Surg.*, vol. 142, pp. 511–516, 2011, doi: 10.1016/j.jtcvs.2011.01.030.

[28] C. Pizarro, R. R. Davies, E. Woodford, and W. A. Radtke, "Improving early outcomes following hybrid procedure for patients with single ventricle and systemic outflow obstruction: defining risk factors," *Eur. J. Cardio-Thoracic Surg.*, vol. 47, no. 6, pp. 995–1001, Jun. 2015, doi: 10.1093/EJCTS/EZU373.

[29] J. R. Dillman, A. L. Dorfman, A. K. Attili, P. P. Agarwal, A. Bell, G. C. Mueller, R. J. Hernandez, "Cardiovascular magnetic resonance imaging of hypoplastic left heart syndrome in children," *Pediatr. Radiol.*, vol. 40, no. 3, pp. 261–274, Mar. 2010, doi: 10.1007/S00247-009-1473-5/TABLES/2.

[30] P. Lamata, M. Sinclair, E. Kerfoot, A. Lee, A. Crozier, B. Blazevic, S. Land, A. J. Lewandowski, D. Barber, S. Niederer, N. Smith, "An accurate, fast and robust method to generate patient-specific cubic Hermite meshes," *Med. Image Anal.*, vol. 15, no. 6, pp. 801–813, Dec. 2011, doi: 10.1016/J.MEDIA.2011.06.010.

[31] K. Gilbert, N. Forsch, S. Hegde, C. Mauger, J. H. Omens, J. C. Perry, B. Pontré, A. Suinesiaputra, A. A. Young, A. D. McCulloch, "Atlas-based computational analysis of heart shape and function in congenital heart disease," *J. Cardiovasc. Transl. Res.*, vol. 11, no. 2, pp. 123–132, 2018, doi: 10.1007/s12265-017-9778-5.

[32] K. Gilbert, N. Forsch, S. Hegde, C. Mauger, J. H. Omens, J. C. Perry, B. Pontré, A. Suinesiaputra, A. A. Young, A. D. McCulloch, "Atlas Based Computational Analysis of Heart Shape and Function in Congenital Heart Disease HHS Public Access," *J Cardiovasc Transl Res*, vol. 11, no. 2, pp. 123–132, 2018, doi: 10.1007/s12265-017-9778-5.

[33] R. Chandrashekara, R. Mohiaddin, R. Razavi, and D. Rueckert, "Nonrigid image

registration with subdivision lattices: application to cardiac MR image analysis," *Med. Image Comput. Comput. Assist. Interv.*, vol. 10, no. Pt 1, pp. 335–342, 2007, doi: 10.1007/978-3-540-75757-3_41.

[34] R. V. Stebbing, A. I. L. Namburete, R. Upton, P. Leeson, and J. A. Noble, "Data-driven shape parameterization for segmentation of the right ventricle from 3D+t echocardiography," *Med. Image Anal.*, vol. 21, no. 1, pp. 29–39, Apr. 2015, doi: 10.1016/J.MEDIA.2014.12.002.

[35] C. Mauger, K. Gilbert, A. Suinesiaputra, J. Omens, A. Mcculloch, and A. Young, "An Iterative Diffeomorphic Algorithm for Registration of Subdivision Surfaces: Application to Congenital Heart Disease", doi: 10.1109/EMBC.2018.8512394.

[36] A. H. Schultz, J. Kreutzer, "Cyanotic Heart Disease," *Pediatr. Cardiol.*, pp. 51–78, Jan. 2006, doi: 10.1016/B978-0-323-02367-2.50010-9.

[37] J. Stam, "Exact Evaluation Of Catmull-Clark Subdivision Surfaces At Arbitrary Parameter Values".

[38] K. Gilbert, B. R. Cowan, A. Suinesiaputra, C. Occleshaw, A. A. Young, "Rapid D-Affine Biventricular Cardiac Function with Polar Prediction," *Lect. Notes Comput. Sci. (including Subser. Lect. Notes Artif. Intell. Lect. Notes Bioinformatics)*, vol. 8674 LNCS, no. PART 2, pp. 546–553, 2014, doi: 10.1007/978-3-319-10470-6_68.

[39] C. A. Mauger, S. Govil, R. Chabiniok, K. Gilbert, S. Hegde, T. Hussain, A. D. McCulloch, C. J. Occleshaw, J. H. Omens, J. C. Perrym K. Pusharajah, A. Suinesiaputra, L. Zhong, A. A. Young, "Right-left ventricular shape variations in tetralogy of Fallot: associations with pulmonary regurgitation," *J. Cardiovasc. Magn. Reson.*, vol. 23, no. 1, pp. 1–14, Dec. 2021, doi: 10.1186/S12968-021-00780-X/TABLES/4.

[40] E. Zacur, J. Wong, R. Razavi, T. Geva, G. Greil, and P. Lamata, "Revealing Differences in Anatomical Remodelling of the Systemic Right Ventricle," 2015, doi: 10.1007/978-3-319-20309-6_12.

[41] C. A. Mauger, S. Govil, R. Chabiniok, K. Gilbert, S. Hegde, T. Hussain, A. D. McCulloch, C. J. Occleshaw, J. H. Omens, J. C. Perrym K. Pusharajah, A. Suinesiaputra, L. Zhong, A. A. Young, "Right-left ventricular shape variations in tetralogy of Fallot: associations with pulmonary regurgitation," *J. Cardiovasc. Magn. Reson.*, vol. 23, no. 1, pp. 1–14, 2021, doi: 10.1186/s12968-021-00780-x.

[42] A. Crucean, A. Alqahtani, D. J. Barron, W. J. Brawn, R. V. Richardson, J. O'Sullivan, R. H. Anderson, D. J. Henderson, B. Chaudhry, "Re-evaluation of hypoplastic left heart syndrome from a developmental and morphological perspective," *Orphanet J. Rare Dis.*, vol. 12, no. 1, Aug. 2017, doi: 10.1186/S13023-017-0683-4.

[43] K. Fricke, M. Mellander, K. Hanséus, P. K. Tran, M. Synnergren, J. J. Ramgren, A. Rydberg, J. Sunnegårdh, M. Dalén, G. Sjöberg, C. G. Weismann, Liuba, Petru, "Impact of Left Ventricular Morphology on Adverse Outcomes Following Stage 1 Palliation for Hypoplastic Left Heart Syndrome: 20 Years of National Data From Sweden," *J. Am. Heart Assoc.*, vol. 11, no. 7, p. 22929, Apr. 2022, doi: 10.1161/JAHA.121.022929/FORMAT/EPUB.

[44] J. Wong, P. Lamata, R. H. Rathod, S. Bertaud, N. Dedieu, H. bellsham-Revell, K. Pushparajahm, R. Razavi, T. Hussain, T. Schaeffter, A. J. Powell, T. Geva, G. F. Greil, "Right ventricular morphology and function following stage I palliation with a modified Blalock-Taussig shunt versus a right ventricle-to-pulmonary artery conduit," *Eur. J. Cardiothorac. Surg.*, vol. 51, no. 1, pp. 50–57, 2017, doi: 10.1093/ejcts/ezw227.

[45] A. P. Wang, A. M. Kelle, M. Hyun, C. L. Reece, P. M. Young, P. W. O'Leary, M. Y. Qureshi, T. J. Nelson, D. T. haile, A. R. Miller, S. E. Martineau, A. L. Breuer, K. S. Miller, L. A. Riess, K. M. Cavanaugh, L. Timmons, "Negative Impact of the Left Ventricular Remnant Morphology on Systemic Right Ventricular Myocardial Deformation in Hypoplastic Left Heart Syndrome," *Pediatr. Cardiol.*, vol. 42, no. 2, pp. 278–288, Feb. 2021, doi: 10.1007/S00246-020-02480-2.

[46] K. Laohachai, D. Winlaw, G. Sholler, S. Veerappan, A. Cole, and J. Ayer, "The Degree of Left Ventricular Hypoplasia Is Associated with Tricuspid Regurgitation Severity in Infants with Hypoplastic Left Heart Syndrome," *Pediatr. Cardiol.*, vol. 40, no. 5, pp. 1035–1040, Jun. 2019, doi: 10.1007/S00246-019-02111-5/FIGURES/2.

[47] A. A. Taha and A. Hanbury, "An Efficient Algorithm for Calculating the Exact Hausdorff Distance," *IEEE Trans. Pattern Anal. Mach. Intell.*, vol. 37, no. 11, pp. 2153–2163, Nov. 2015, doi: 10.1109/TPAMI.2015.2408351.

[48] O. U. Aydin, A. A. Taham A. Hilber, A. A. Khalil, I. Galinovic, J. B. Fieback, D. Frey, V. I. Madai, "On the usage of average Hausdorff distance for segmentation performance assessment: hidden error when used for ranking," *Eur. Radiol. Exp.*, vol. 5, no. 1, pp. 1–7, Dec. 2021, doi: 10.1186/S41747-020-00200-2/FIGURES/2.

[49] H. Chui and A. Rangarajan, "A new point matching algorithm for non-rigid registration".

[50] G. Farrar, A. Suinesiaputra, K. Gilbert, J. C. Perry, S. Hegde, A. Marsden, A. A. Young, J. H. Omens, A. D. McCulloch, "Atlas-based ventricular shape analysis for understanding congenital heart disease," *Prog. Pediatr. Cardiol.*, vol. 43, pp. 61–69, 2016, doi: 10.1016/j.ppedcard.2016.07.010.

[51] P. Medrano-Gracia, B. R. Cowan, B. Ambale-Venkatesh, D. A. Bluemke, J. Eng, J. P. Finn, C. G. Fonseca, J. A. Lima, A. Suinesiaputra, A. A. Young, "Left ventricular shape variation in asymptomatic populations: the multi-ethnic study of atherosclerosis," 2014, doi: 10.1186/s12968-014-0056-2.

[52] R. R. Arnold, T. Loukanov, and M. Gorenflo, "Hypoplastic left heart syndrome – unresolved issues," 2014, doi: 10.3389/fped.2014.00125.

[53] J. A. Feinstein, D. W. Benson, A. M. Dubin, M. S. Cohen, D. M. Maxey, W. T. Mahle, E. Pahl, J. Villafae, A. B. Bhatt, L. F. Peng, B. A. Johnson, A. L. Marsden, C. J. Daniels, N. A. Rudd, C. A. Caldarone, K. A. Mussatto, D. L. Morales, D. D. Ivy, J. W. Gaynor, J. S. Tweddell, B. J. Deal, A. K. Furck, G. L. Rosenthal, R. G. Ohye, N. S. Ghanayem, J. P. Cheatham, W. Tworetzky, G. R. Martin, "Hypoplastic Left Heart Syndrome: Current Considerations and Expectations," *J. Am. Coll. Cardiol.*, vol. 59, no. 1 Suppl, p. S1, Jan. 2012, doi: 10.1016/J.JACC.2011.09.022.

[54] L. M. Kanngiesser, S. Freitag-Wolf, S. B. Grazioh, D. D. Gabbert, J. H. Hansen, A. S. Uebing, I. Voges, "Serial Assessment of Right Ventricular Deformation in Patients With Hypoplastic Left Heart Syndrome: A Cardiovascular Magnetic Resonance Feature

Tracking Study," *J. Am. Heart Assoc.*, vol. 11, no. 9, p. 25332, May 2022, doi: 10.1161/JAHA.122.025332.

APPENDIX

Appendix 1. Patient-specific Models Created for the HLHS Dataset (ED models first followed by ES models)

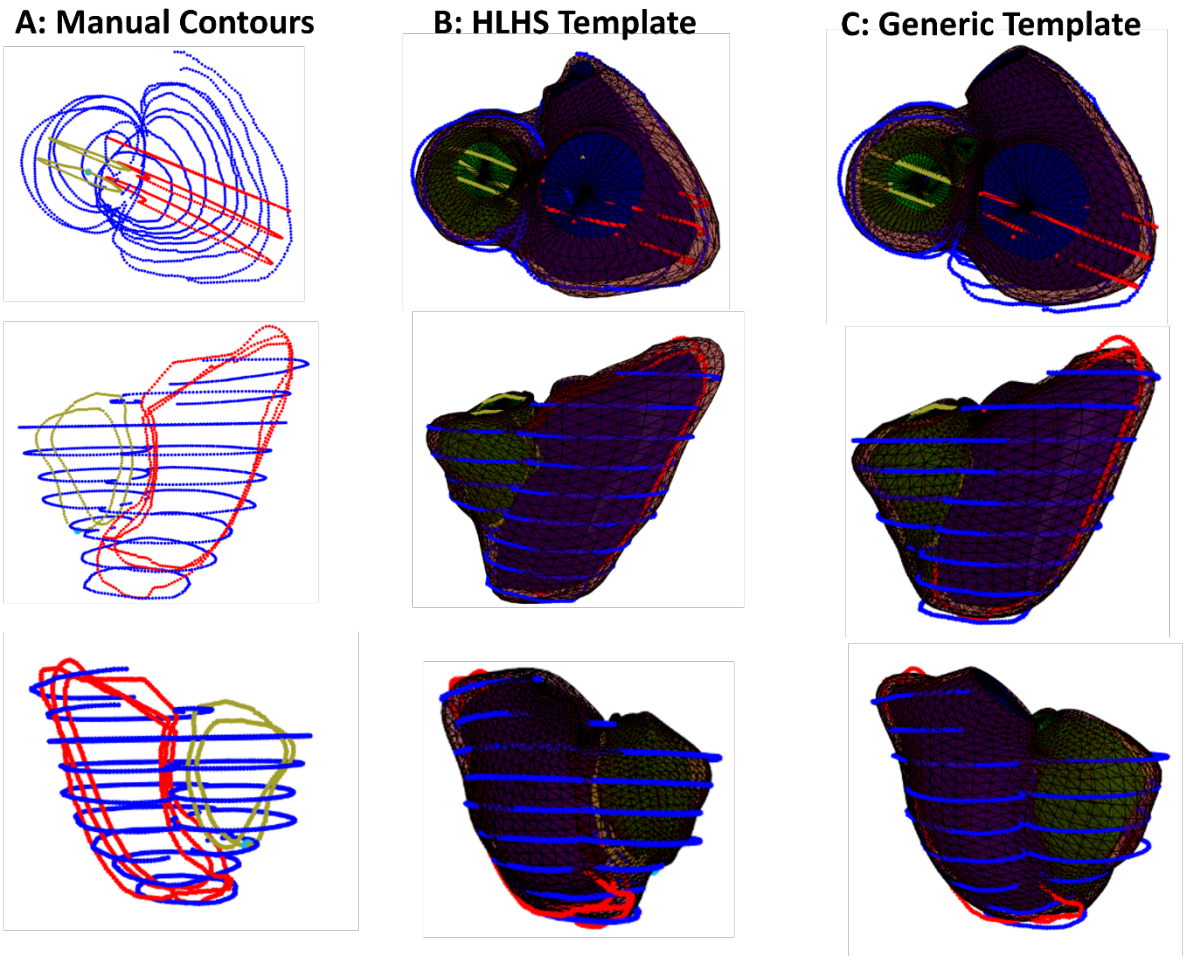

Figure 7.1: Case 1 at End Diastole Models (Blue: epicardium contours, Red: long axis RV endocardium contours, Green: long axis LV endocardium contours, Light Blue: LV apex point)

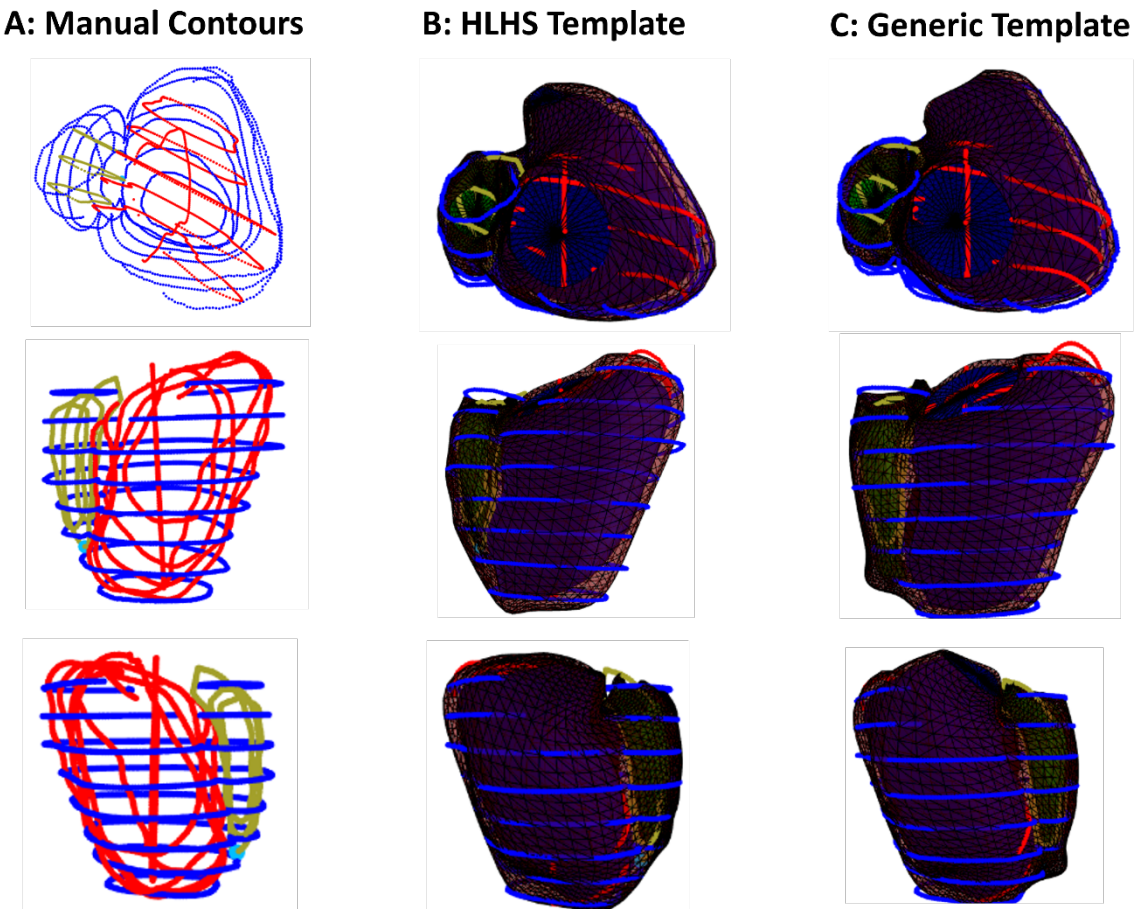

Figure 7.2: Case 2 at End Diastole Models (Blue: epicardium contours, Red: long axis RV endocardium contours, Green: long axis LV endocardium contours, Light Blue: LV apex point)

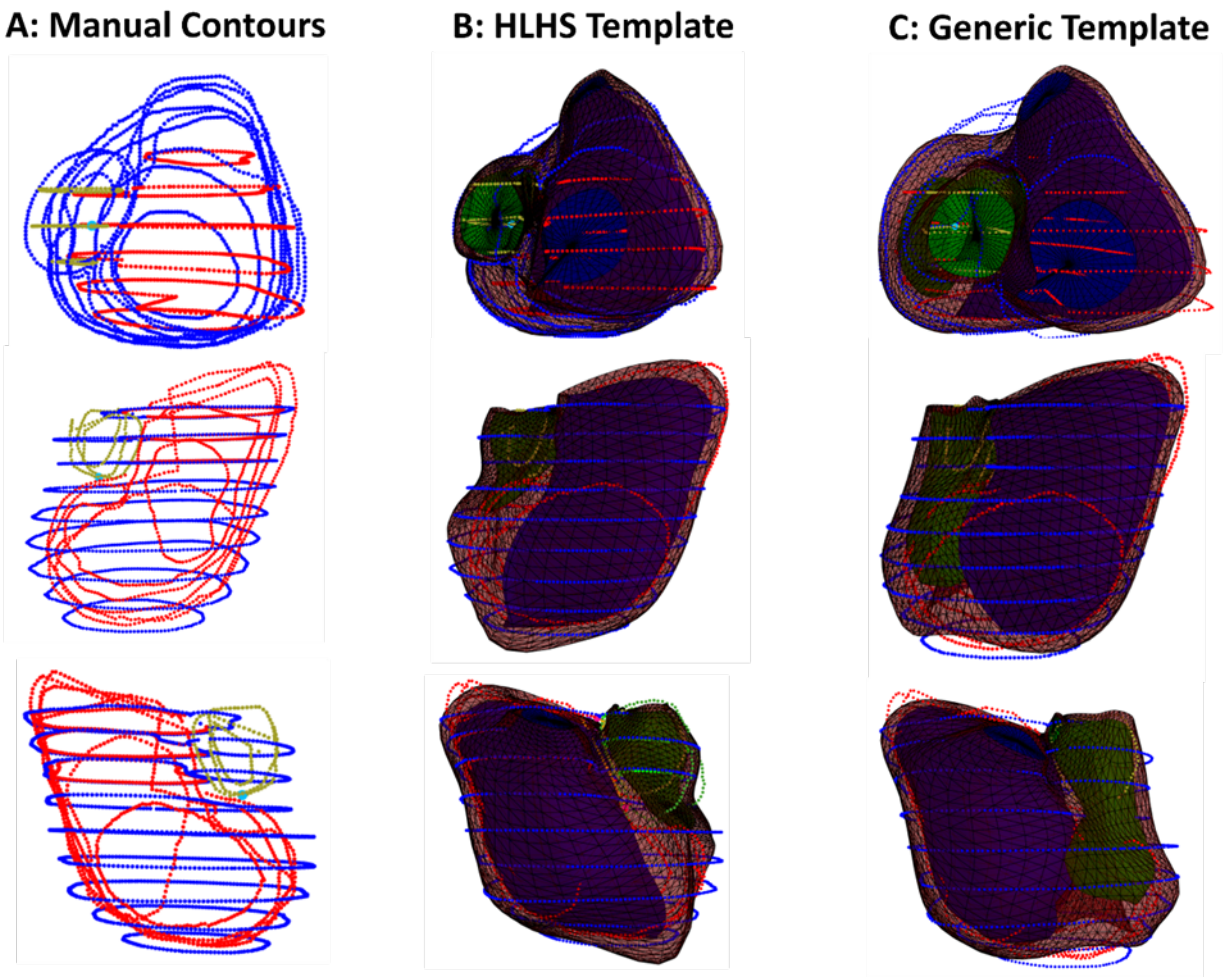

Figure 7.3: Case 3 at End Diastole Models (Blue: epicardium contours, Red: long axis RV endocardium contours, Green: long axis LV endocardium contours, Light Blue: LV apex point)

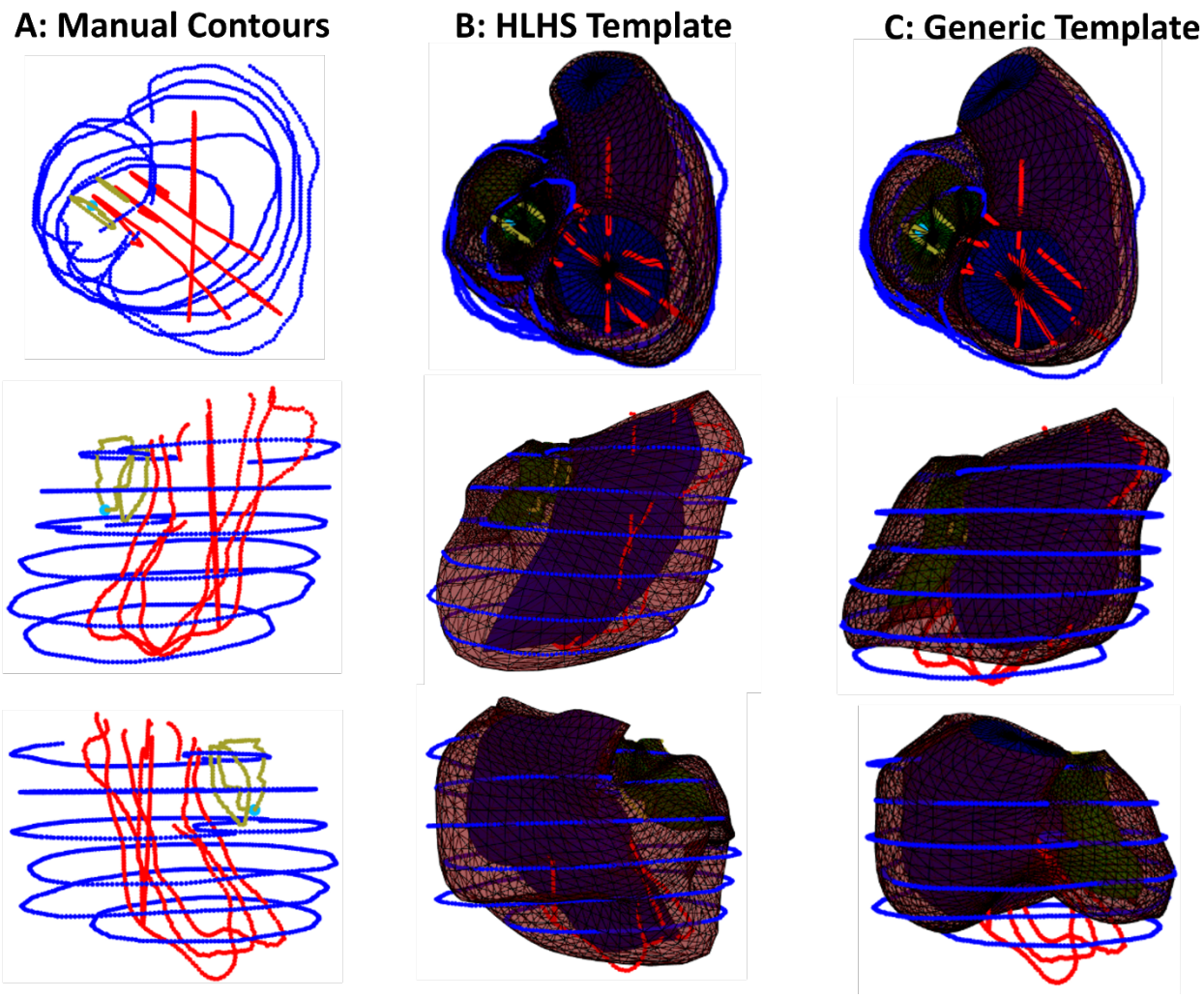

Figure 7.4: Case 5 at End Diastole Models (Blue: epicardium contours, Red: long axis RV endocardium contours, Green: long axis LV endocardium contours, Light Blue: LV apex point)

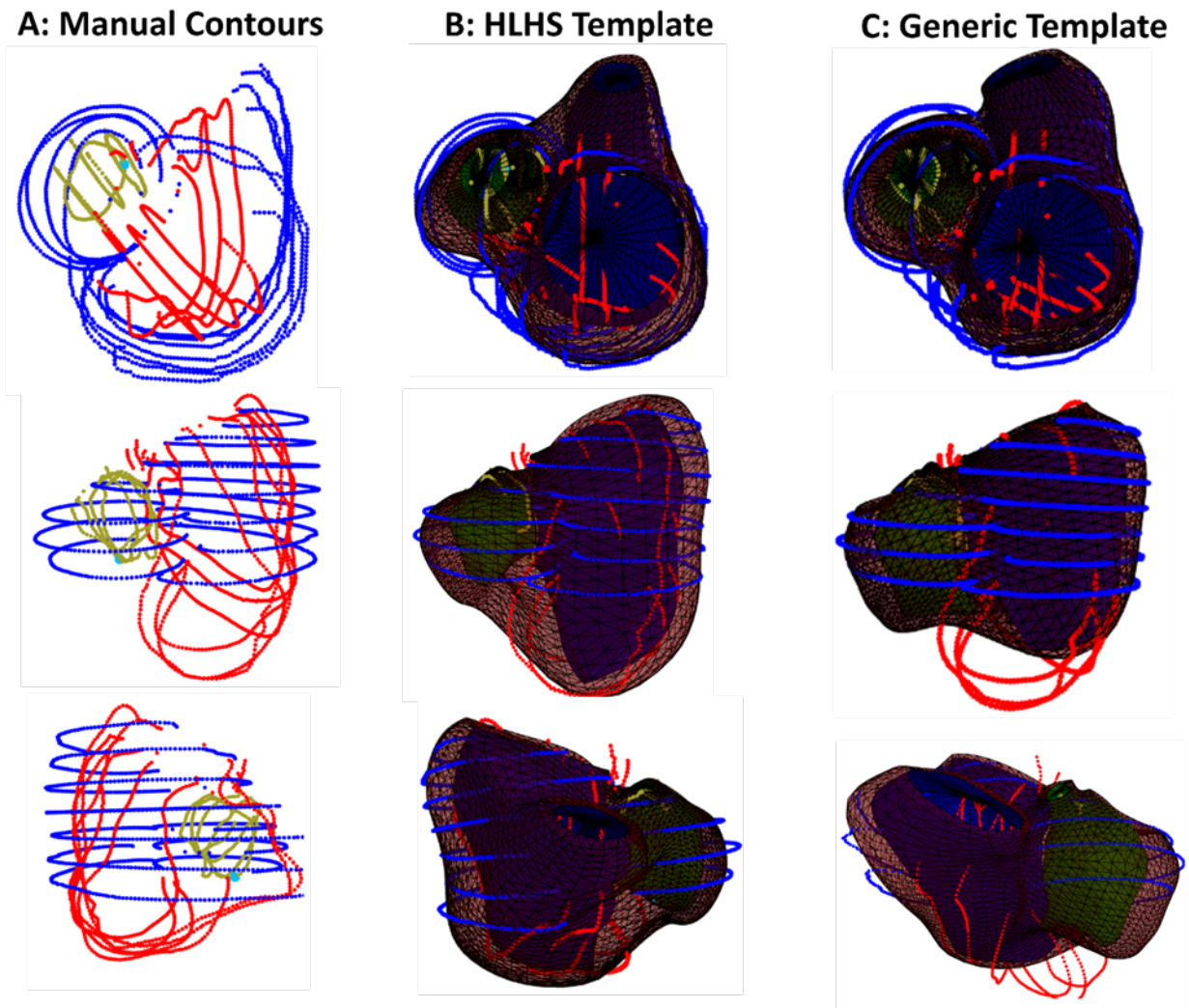

Figure 7.5: Case 6 at End Diastole Models (Blue: epicardium contours, Red: long axis RV endocardium contours, Green: long axis LV endocardium contours, Light Blue: LV apex point)

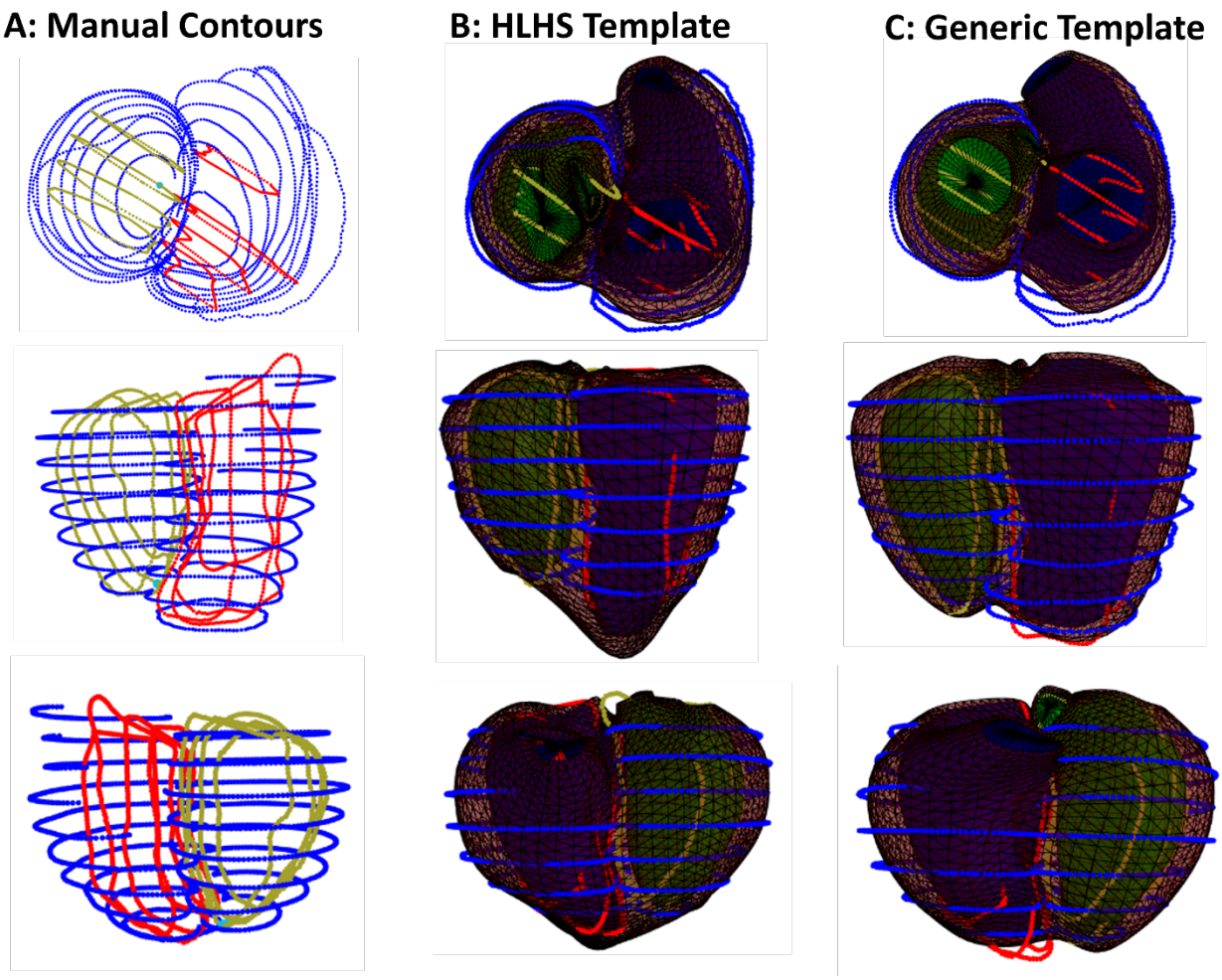

Figure 7.6: Case 4 at End Systole Models (Blue: epicardium contours, Red: long axis RV endocardium contours, Green: long axis LV endocardium contours, Light Blue: LV apex point)

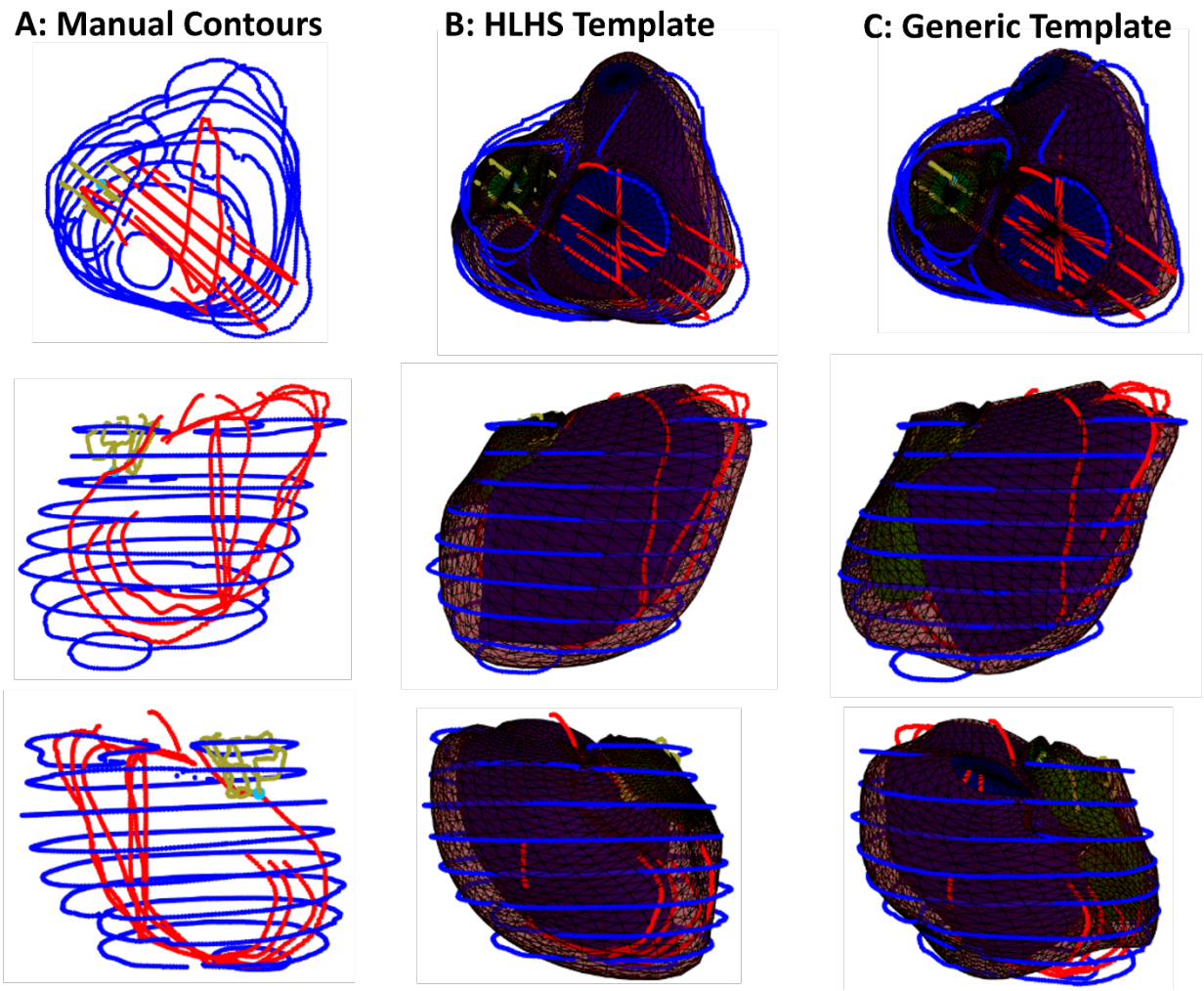

Figure 7.7: Case 5 at End Systole Models (Blue: epicardium contours, Red: long axis RV endocardium contours, Green: long axis LV endocardium contours, Light Blue: LV apex point)

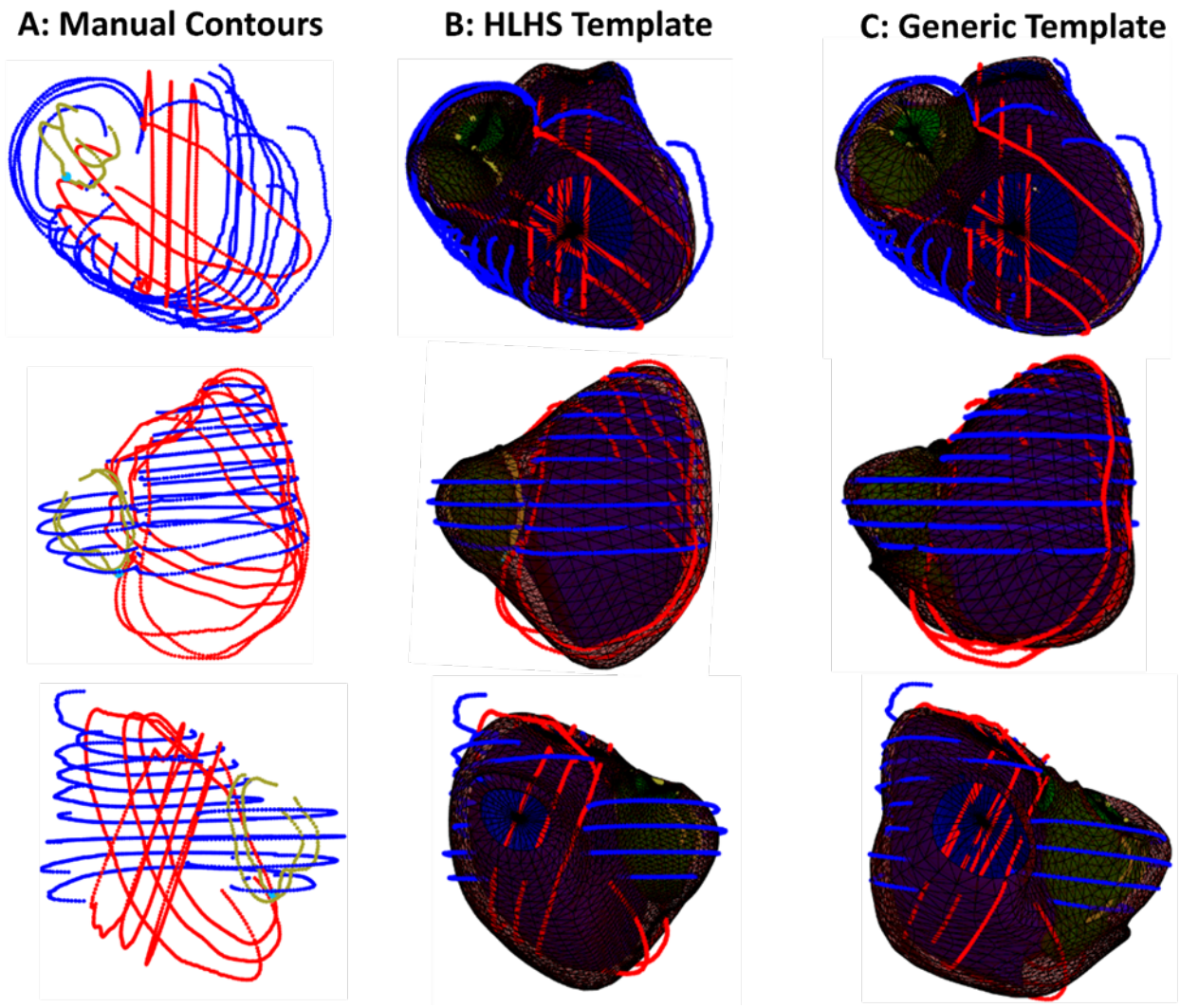

Figure 7.8: Case 6 at End Systole Models (Blue: epicardium contours, Red: long axis RV endocardium contours, Green: long axis LV endocardium contours, Light Blue: LV apex point)